

Mapping West Virginia Surface Mines with Hyperspectral Remotely Sensed
Imagery Classification

by

Alexander Edward Zoeller

A Thesis Presented to the
Faculty of the USC Graduate School
University of Southern California
In Partial Fulfillment of the
Requirements for the Degree
Master of Science
(Geographic Information Science and Technology)

August 2017

Copyright © 2017 by Alexander Edward Zoeller

For Lara, with all my love.

Table of Contents

List of Figures	vi
List of Tables	vii
Acknowledgements	viii
List of Abbreviations	ix
Abstract	xi
Chapter 1 Introduction	1
1.1 Mapping Surface Mining	2
1.2 Classification of Remotely Sensed Imagery	4
1.3 Study Area	5
Chapter 2 Related Work.....	8
2.1 Background	8
2.2 Hyperspectral Image Classification	13
2.3 Classifying Minerals and Mine Operations with AVIRIS Data	16
2.4 Impact of Legislation and Role of Spatial Data Analysis	19
Chapter 3 Methods	20
3.1 Data Preparation.....	20
3.1.1. Data Integration	20
3.1.2. Data Quality	23
3.1.3. Data Preparation.....	24
3.2 Classification.....	27
3.3 Spatial Analysis	29
Chapter 4 Results	31
4.1 Data Quality Inspections	34
4.1.1. Horizontal Accuracy	34
4.1.2. Atmospheric Distortion.....	39
4.2 Results of Classification	40
Chapter 5 Discussion	47
5.1 Future Work	49

5.2 Further Research	52
5.3 Applications of Research	53
REFERENCES	58

List of Figures

Figure 1 Surface coal mining operation in West Virginia.....	3
Figure 2 The study area in southern West Virginia6
Figure 3 Landsat 5 (Thematic Mapper) image9
Figure 4 Pixel luminance value example	10
Figure 5 Landsat TM light collection overview	12
Figure 6 Soil composition classification based on AVIRIS flight data	17
Figure 7 Surface mineral classification.....	18
Figure 8 An example of three different surface mines	24
Figure 9 Automated classification returns.....	32
Figure 10 Supervised classification returns	33
Figure 11 Views of GPS reference station.....	35
Figure 12 CORS precise coordinates	36
Figure 13 Autocorrelation analysis in screen function	39
Figure 14 Output of hyperabsorb function in automated classification.....	41
Figure 15 Output polygon from automated classification over 3D model	42
Figure 16 Results of automated surface mine classification	44
Figure 17 Results of supervised classification	45
Figure 18 “False returns” in automated surface mine classification.....	46
Figure 19 Subset of study area with representation of flow directions	51

List of Tables

Table 1 Data requirements	22
Table 2 AVIRIS dataset horizontal accuracy assessment.....	38
Table 3 Results of classifications and false return rates.....	47

Acknowledgements

I would like to acknowledge the tireless effort and support that my advisor Steven Fleming provided. I would never have been able to complete this project without your help and guidance along the way, as well as for the coursework you guided me through that contributed to the idea for this study. I would like to thank my instructor Elizabeth Sedano for helping me turn my dreams for this thesis into a reality. I would like to thank my former manager, Derwin Cantrell, for his support of my educational goals and the care he has showed me during difficult times. I would also like to express gratitude to Sarah Lundeen at NASA's Jet Propulsion Laboratory, for helping me acquire the hyperspectral data required to perform this study. Finally, I would like to thank my parents for all their love and support, and for the crucial help of my mentor Ron Oshima.

List of Abbreviations

AO	Area of Operations
ASTER	Advanced Spaceborne Thermal Emission and Reflectance Radiometer
AVIRIS	Airborne Visible / Infrared Imaging Spectrometer
CORS	Continually Operating Reference Station
CRS	Coordinate Reference System
DEM	Digital Elevation Model
DN	Digital Number
ETM	Enhanced Thematic Mapper
FTP	File Transfer Protocol
GDAL	Geospatial Data Abstraction Library
GIS	Geographic information system
ISR	Intelligence, Surveillance and Reconnaissance
JPL	Jet Propulsion Laboratory
NAD	North American Datum
NAIP	National Agriculture Imagery Program
NGS	National Geodetic Survey
OSM	Office of Surface Mining
RSR	Relative Spectral Response
SAM	Spectral Area Mapping
SDE	Spectral Discriminatory Entropy
SDP	Spectral Discriminatory Probability
SID	Spectral Information Divergence

SSI	Spatial Sciences Institute
SRTM	Shuttle Radar Topographic Mission
TM	Thematic Mapper
USC	University of Southern California
USGS	United States Geological Survey
UTM	Universal Transverse Mercator
UXO	Unexploded Ordinance
WGS	World Geodetic System

Abstract

Mapping surface mines and mine activity is integral to both environmental preservation and tracking industrial production. West Virginia has a long history of coal and other types of surface mining, but detailed spatial information representing the extent of operations is limited. In developing nations, such information often does not exist in any form. While field collections of spatial feature data relating to mine activity are costly and resource-intensive, remotely sensed imagery presents a readily available tool to identify and map surface mines and their footprints on the Earth's surface.

Geographically referenced raster image datasets from sensors on board satellites in space as well as airborne vehicles can represent wavelengths of light well beyond the range of the visible spectrum. These types of multispectral datasets present grids of cells on the Earth's surface that each represent the luminance properties of the surface materials *at clearly defined wavelengths of light*. This study analyzed recently collected multispectral data from West Virginia by examining the reflectance values at each point on the ground and attempted to classify materials known to exist in high concentrations in large mounds or pilings that are typically adjacent to large-scale surface mines. By inputting the known spectral properties of these Earth minerals into the classification process, this study was able to automatically classify and map the signature features of surface mines without user input or analysis. The automated classification methodology developed and tested in this study accurately identified surface mine locations throughout the study area in West Virginia at a rate of over 98%, and the output feature dataset can be implemented immediately in a comprehensive impact study of mining operations on the surrounding environment and populations.

Chapter 1 Introduction

Surface mines pose a grave risk to human populations. Surface mines introduce harmful mineral elements and other toxins into local drainage networks as well as the air, and contribute directly to higher rates of a variety of illnesses in local populations. Alarming, areas designated as situated in surface mining zones in Appalachia have a 63% greater rate of birth defects in newborns (Ahern 2011). By 2005, surface mining represented 5% of the total surface area of southern West Virginia (Bernhardt 2012). As the industrial practice of surface mining – and especially coal mining – continues to progress, industrial processes pose a significant risk to natural resources and the local environment. Whether the growth rate of mining operations increases or decreases in each year, newer mines opening, as well as continuing excavation on existing mines, mean that there is a greater concentration of mineral elements uprooted from underneath the Earth's surface and deposited primarily in nearby stream valleys (Bernhardt 2012).

This thesis classifies and maps these pilings of unearthed soils and minerals by incorporating elements of established methodologies, and utilizing geographically referenced raster data collected from aerial scanners mounted on aircraft. While such camera systems take many forms, and produce a wide array of different raster datasets, this study utilizes orthorectified, hyperspectral raster data that is both accurate (in terms of geographic reference) and representative of a wide and clearly defined range of light. The classifications conducted in this study interpret reflected light from the ground at specifically defined geographic points, thereby differentiating the tell-tale mineral pilings surrounding surface mines. From this, it is possible to represent these mines in a GIS for further analysis. Such an approach serves to

address a glaring gap in existing spatial data relating to surface mine activities in the United States, and to address a complete lack of such data in many developing countries.

1.1 Mapping Surface Mining

“Valley fills” are large pilings of unearthed soil that are taken from surface mines (often situated at the top of a hill due to a higher concentration of valuable minerals) and deposited into nearby basins. Such pilings occupy a significant amount of space. In 2007, they covered an estimated 25,178 acres in West Virginia, which exceeds 100 square kilometers (Burns 2007). The fact that these remnants of surface mining activity are deposited in valleys surrounding the hills being mined represents a major threat to the environment, as the mineral-rich contents of these pilings often alter the pH of streams and river networks that traverse these valleys (see Figure 1). Acidification of the local stream networks and the entire watershed is just one major environmental hazard posed by these surface mines as a direct result of sulfides and numerous other minerals in the unearthed soil pilings oxidizing and draining into rivers (Blahwar 2012; Khalil 2014). Surface mines also continue to pose a significant threat to the environment after they become abandoned or merely inactive, because these mineral pilings remain exposed.



Figure 1 Surface coal mining operation in southern West Virginia. Tell-tale pilings of unearthened mineral elements surround the site, especially in depressed valleys around hilltop mines (Image Source: The Columbus Dispatch, July 20, 2014)

Resources available for mapping and monitoring these mines as well their respective footprints on the surface are limited. While state and federal agencies such as the Office of Surface Mining (OSM) maintain spatial databases relating to active and inactive mine locations, they do not track or monitor the size or footprint of surface mines. Political pressure from the industry, social pressure from a population that relies on the industry, as well as financial constraints restrict the ability of environmental protection agencies to conduct field studies in which laboratory samples and photographs of mine sites are collected regularly (Burns 2007).

Remotely sensed imagery presents an invaluable tool for assessing and monitoring these types of surface mining operations. Orthorectified imagery from both satellite-based and aerial sensor platforms has been used to analyze the Earth's surface to identify mines and establish the presence of either valuable or hazardous minerals (Adep 2016; Charou 2010; Clark 1999; Dalton 2004 & 2007; Khalili 2015; Kruse 1993; Rockwell 2012; Zhang 2012). While image-based spatial datasets are typically coarse in resolution due to the large distances between the sensors

and the ground, surface mines are unique in that their signatures (that is, the large pilings of minerals and soils around their sites) are relatively large, and can therefore be detected even in datasets where pixels (the cells that make up an image representation) might measure 30 meters of ground sampled distance when measured on the Earth's surface.

1.2 Classification of Remotely Sensed Imagery

This study tested a methodology that incorporates existing research into classifications of surface materials identified in geographically referenced and orthorectified raster image datasets. The classification of raster imagery in this study was used to detect the presence of large mineral pilings near surface mines automatically. Orthorectified image sources have been corrected to account for the changing shape of the Earth's surface, which is typically accomplished by stretching and compressing parts of the image to link known control points in the captured image with a corresponding point in an established reference image. By linking these geographically defined spatial points in collected images and creating a final orthorectified layer, an image dataset can be imported into a Geographic Information System (GIS) and used to precisely measure elements on the Earth's surface at the time that the image was collected.

Classification of images has evolved significantly over the years that remotely sensed spatial data has been available. While traditional classification methods involved manually counting features in an aerial photograph captured from a balloon or airplane, computer algorithms that have the capacity to identify and differentiate materials and elements (not just features) can facilitate and automate the entire process. For the study of surface mines, in which ground reconnaissance is extremely difficult, if not impossible, due to limited resources, an effective and accurate classification methodology fills a glaring need in monitoring activities that pose a grave environmental risk.

1.3 Study Area

The study area represents a high concentration of surface mining activity, both historical and current, and is ideally suited for this study based both on the availability of hyperspectral imagery data as well as the glaring need to map mines and measure the potential impact on surrounding populations. The study area, shown in Figure 2, is situated in the southeastern region of West Virginia in the Appalachian Mountains, and measures 2633.5 square kilometers. The population residing within the study area in 2010 is 47,705, according to the US Census Bureau. There are 340 total surface mines in the study area, and of these 52 were active between 2000 and 2011, when the hyperspectral imagery was collected.

This study utilized raster data collected from the Airborne Visible/Infrared Radiometer and Spectrometer (AVIRIS), which was designed and is maintained by NASA's Jet Propulsion Laboratory (JPL). The AVIRIS sensor is mounted on an airplane and flown in swaths over planned collection areas; the data is therefore expensive to collect. Because of the density of the data, it is labor-intensive to process into a final deliverable raster layer that can be imported into a GIS. Such data is therefore limited in terms of its availability and coverage for specific geographic areas. In West Virginia, only four AVIRIS flights have been flown. Of these, the most recent flight and the one from which the largest area coinciding with surface mine locations was flown in July 2009. The study area was selected to match the area covered by this recent AVIRIS dataset. It extends from the northeast of West Virginia to the south, and as reported by the OSM in 2010 includes 340 active and inactive surface mines, of which 52 were in active operation between the year 2000 and 2011.

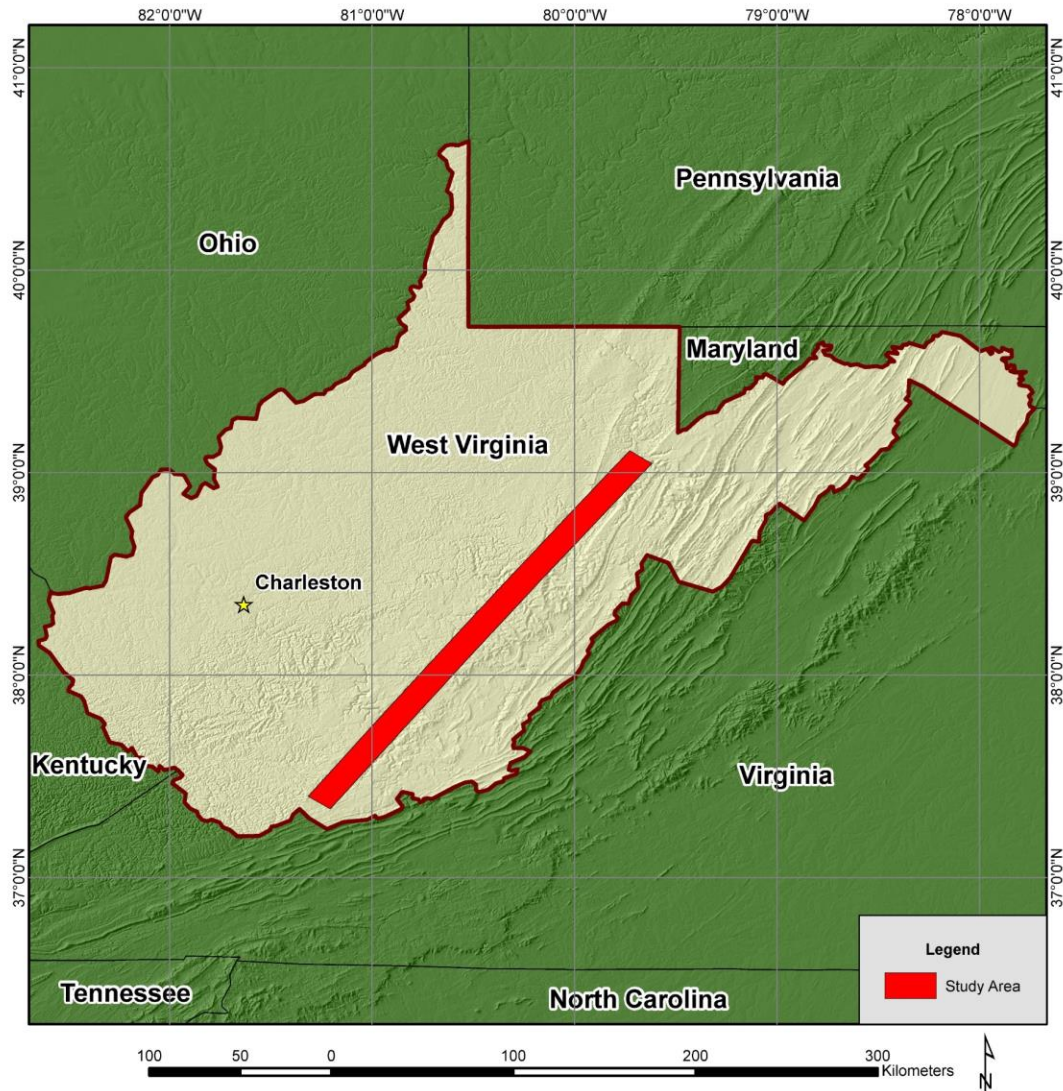


Figure 2 The study area in West Virginia. Entire area is represented in AVIRIS hyperspectral image dataset collected July 14, 2009

What follows is a summary of background research relating to remotely sensed imagery, raster data analysis, classification, and identifying different mineral elements from such analyses. A fundamental analysis of the nature of spatially referenced raster datasets is essential to understanding the possibilities for geostatistical algorithms capable of classifying surface materials. A detailed description of numerous studies into classification methodologies applied to AVIRIS hyperspectral datasets representing areas of heavy mining operations follows. The

methodologies utilized in this study were shaped by the efficacy of earlier approaches. The methodology employed by this study is described in detail, and the results of the study as well as required further analysis follow.

Chapter 2 Related Work

Academic and professional studies that explore classification methodologies are often made possible by a historical body of work relating to photogrammetry principles concerning orthorectification of remotely sensed ground observation and photoradiometric principles concerning the capture of reflected light off the ground by aerial camera systems (Clark 1990; Clark 1991; Dutta 2015; Heinzl 2006; Rockwell 2010). These two distinct but interrelated principles need to be understood to approach any methodology related to classification of digital raster images. As such, they are discussed in the opening section of this chapter, before a detailed description of how these principles apply to AVIRIS datasets specifically can follow. Finally, this chapter explores how classification methods incorporating hyperspectral raster data have been utilized to effectively map mining operations in different parts of the world.

2.1 Background

While spatial data representing surface mines in West Virginia exist, detailed maps representing the spatial distribution of unearthed minerals do not. Further, maps representing mines (as well as unearthed minerals) in many countries do not exist; this represents a challenge not just for conservation efforts but also for government oversight and corporate management of mining operations. Remote sensing by airborne sensors mounted on fixed-wing aircraft provide previously unattainable capabilities towards mapping the presence and distribution of surface mines. NASA's AVIRIS sensor provides the ability to detect specific spectral signatures from known minerals, soils, vegetation, and other surface materials at a well-defined spectral range. The datasets returned from AVIRIS collections provide the capability to classify the imagery, and create a rasterized map of a given area representing every surface material as a different

value. This eliminates the requirement to deploy researchers to the field to collect samples and study them in a laboratory.

Much previous work has been focused on classifying images from the AVIRIS sensor. Previous studies have worked to develop classification algorithms that can identify what type of material is present at each precise location in a given raster grid (Clark 1999; Dalton 2004; Kruse 1993; Mars 2003; Rockwell 2005). In short, each image is divided into rows and columns of pixels (or *picture elements*), with each square pixel bounded by precise coordinates on the Earth's surface (see Figure 3). Each pixel, or cell, within the image contains precise data of the light captured by the sensor that was reflected from that specific spot on the ground. For a standard camera that captures light in the visible spectrum in the red, green, and blue bands, each pixel is assigned three values: one for the red band, one for blue, and one for green. These assigned light values typically fall within the 0 – 255 integer values for 8-bit data, where 0 represents black and 255 represents pure white.

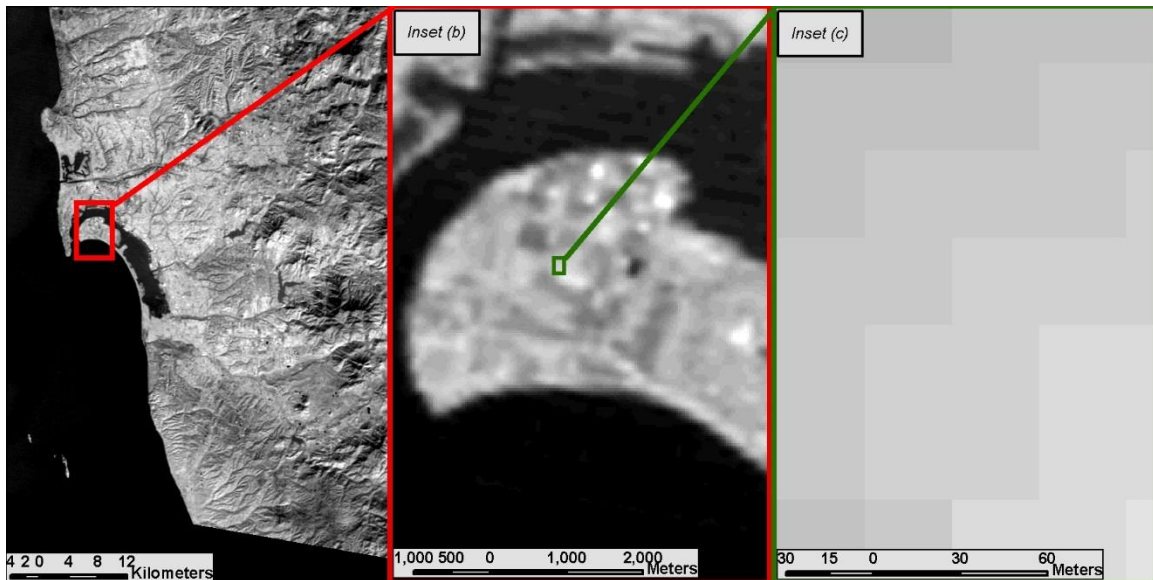


Figure 3 Landsat 5 (Thematic Mapper) image dated 3/13/2011, with larger scale insets (b) and (c) shown to represent pixel composition

The reason that 256 integer values are so commonly used to represent light reflects the design of the computer systems used to process and store the data, where a bit represents either a 1 or a 0, and a byte is made up of eight bits ($2^8 = 256$ possible variations). It is more simple and more conducive to effective processing to represent each light value for each pixel as a single byte, and in extensive historical testing and usage, 256-value light ranges seem to represent adequate diversity for representing and analyzing real-world scenes (Canty 2014). These three band values, taken together, represent a defined color for the pixel represented in the overall picture (Fourest 2012). For black and white (or *panchromatic*) images, the light values are collected along a single defined channel or *band*, typically situated in the middle of the blue, green, and red wavelength range. They are then presented as a 0 to 255 value (representing black to white with shades of grey in between – see Figure 4). With panchromatic greyscale images, as with photo images captured for each of the three visible light wavelength ranges, the black to white light Digital Number (DN) Value from 0 to 255 represents luminance for light collected at each specific pixel location at the time of image capture, and at the wavelength range for the designated band of image capture.

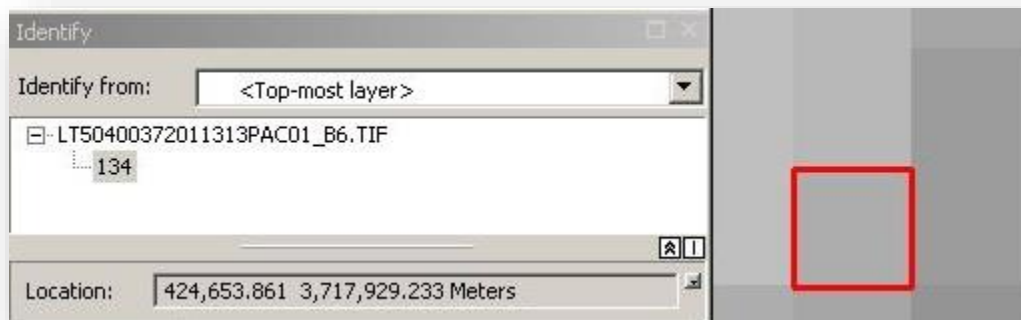


Figure 4 The selected pixel (highlighted in red) represents a greyscale color value with integer value from 0 to 255 for this Landsat TM band 6 image, which is precisely georeferenced to the World Geodetic System (WGS) 1984 Datum, projected to Universal Transverse Mercator (UTM) Zone 11N

AVIRIS data is collected with the same principles of light ranges and color depth, but they contain more detailed definitions. Instead of 8-bit RGB depth typical of both satellite imagery and aerial photography, AVIRIS data picture elements represent 16-bit color depth, which contains 65,535 different possible DN values ($2^{16}-1$) for each pixel at each wavelength (Clark 1990). The imagery spans a *multispectral* range that other more ubiquitous optical sensors cover; common sensor platforms such as the space-borne Landsat system collect similar wavelength ranges, from the blue band at a 400 nanometers (nm) lower bound to the higher-wavelength thermal infrared bands above 2,400 nm. The reason that it is common for so many sensors to capture a similar and broad range of light wavelength channels is that these are the bands at which the vast majority of earth surface materials reflect and absorb light. The term multispectral applies to imagery data such as these that include light values from above wavelength bounds of visible light, and in some cases from below the lower bound of blue light.

The term *hyperspectral* refers to image data stored in raster format that contains data across the full multispectral range, and that is divided into a *larger* number of light channels (Jenson 2007). While satellite imagery such as datasets collected by Landsat and the Advanced Spaceborne Thermal Emission and Reflectance Radiometer (ASTER) can collect broad ranges of spectral data across multiple wavelength band layers that are precisely georeferenced, such image data types are limited in that each band layer contains a relatively large spectral range of light values. The red band (band 3) for Landsat TM data, for example, collects light from the 630 nm to 690 nm wavelength range and represents it as a DN from 0 to 255. While the average and *relative spectral response* for this and other wavelength channels (represented as a georeferenced pixel square in the raster) falls along a relatively narrow range, the overall larger range of each band allows for light reflected at different wavelengths to be perceived as the same or similar

luminance value for that given pixel (Heinzel 2006). Further, there are broad gaps between bands in these satellite image sensors within which many common surface materials (such as soils, minerals, and vegetation) reflect and absorb light. These gaps, as well as the materials that reflect light within those ranges, are demonstrated in Figure 5. A hyperspectral sensor with a significantly higher number of wavelength band layers that collect narrower ranges of light reflectance allow for the *sources* of reflected light –the surface material that is reflecting light back to the sensor – to be more effectively and accurately classified (Dalton 2004).

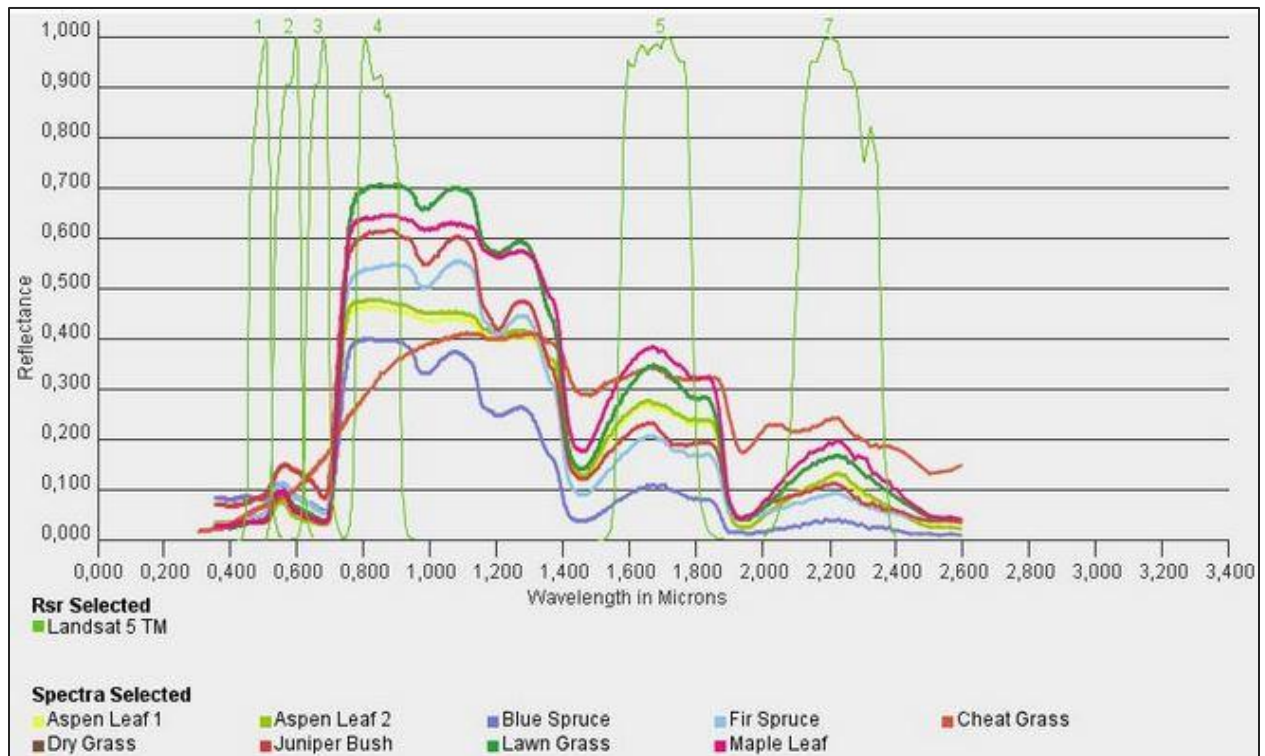


Figure 5 Landsat TM light collection for each of seven separate bands represented in green, while light reflectance and absorption properties for common vegetation types represented to show the difficulty in distinguishing similar surface elements based on multispectral image sensors collected broad ranges of light per layer (Heinzel 2006)

With both AVIRIS raster datasets as well as other types of aerial photography, images are orthorectified in a processing stage prior to delivery to users that typically engage in ecological and other scientific studies. The sensor collects ground images in a push-broom scan, in which a

swath about 20 km wide (depending on the altitude flown) is captured below the aircraft as it travels along a pre-planned line of flight. Aerial imagery captured by the AVIRIS sensor are not captured as a flat projection of the Earth's surface, but rather reflect the elevation relief that makes up the ground itself. Also, the images are not georeferenced until after analysts process them through an orthorectification process (Dalton 2004). The output of these processes is a set of 224 raster layers each representing a narrow band of light, with each containing arrays of pixels corresponding to fixed locations on the ground. This means that for each pixel cell, there are 224 DN integer values each representing how the ground reflected light along the respective light wavelength of that channel. The math operations that have previously been studied are carried out for each cell in the image and for each material in a spectral library (a digital file describing in numeric terms how every known element and mineral reflects light), where the bands at which specific elements reflect or absorb light are represented as number values that are either multiplied or divided. The returned values for each geographically defined cell determine the likelihood of which material is present in that location.

2.2 Hyperspectral Image Classification

Image classification refers to a process that interprets georeferenced surface imagery to map surface composition. Original approaches – such as those developed for use with legacy Landsat data – performed mathematical operations such as *ratios* that divided the DN values for different light bands at the same pixel location, iterated through an entire raster dataset. Ferric minerals, for instance, absorb light at wavelengths about the center of the Landsat TM 7 band. They also reflect light around the center of Landsat TM band 5. This means that for a given pixel that represents iron-rich elements on the ground, the DN return value represented in the band 7 layer at that point will be low, with light absorbed and not reflected, and the DN return value

represented in the band 5 layer will be high (Clark 1999; Dalton 2004). Displaying band 7 for a given geographic area in a typical greyscale – where lower DN returns are presented closer to black and higher DN returns are presented closer to white – will show areas rich in iron elements as white, but they will show other areas as white as well, due to the fact that numerous elements share similar spectral reflectance properties. By creating a new raster layer through geoprocessing that maintains the geometry of geographically referenced rows and columns, but that displays the return of the band 5 value divided by the band 7 value, elements that share reflectance but not absorption properties will be filtered out of the display, accomplishing a rudimentary classification.

With the introduction of hyperspectral imagery, which allowed for a more robust and more stratified range of the light spectrum to be analyzed, algorithms and methodologies have been developed to more accurately estimate the surface composition of a given pixel. Soft or *fuzzy* classification methods interpret larger pixels (such as the 16 m wide AVIRIS data or the 30 m wide Landsat multispectral pixels) and gauge the proportional presence of multiple materials that might be present in a single cell. Classification methods also take into account the DN values for neighboring cells to better differentiate surface materials (Yao-hua 2012). Spectral Area Mapping (SAM), Spectral Discriminatory Probability (SDP), Spectral Discriminatory Entropy (SDE), and Spectral Information Divergence (SID) are all algorithms that have been developed in the 1980s and 1990s to manipulate light reflectance values with an inputted spectral library to classify images sensed across a broad spectrum of light, from the visible blue, green, and red to the infrared and other “hyperspectral” wavelength ranges. Of these, the SID algorithm presents the most effective and accurate method of classifying known mineral elements (Adep 2016). These spectral libraries are digital collections of elements and their respective light

properties (absorption and reflectance), typically calculated by spectrometers in a controlled laboratory. As with the above example of ferric minerals, mathematical operations can be carried out using the DN values for each pixel, and focusing on bands in the light spectrum at which each given material in the spectral library presents unique absorption or reflectance properties.

The USGS Tetracorder system is an algorithm developed to compare sets of light absorption features for given materials based on user-defined variables. Classification methods such as SAM and SID have become accurate as a result of development, but when a specific known mineral is being search for – and the user inputs the light properties of these materials into the algorithm – the Tetracorder algorithm can return a much more accurate classification (Dalton 2004). When an *unsupervised* classification is processed, an output raster layer assigns an integer value relating to a specific material that represents the algorithms best guess for what material is present at that point on the Earth’s surface, or for algorithms that present different layers for each material in a whole spectral library, what normalized proportion that material makes up in that cell. For the latter forms of classifications, if a spectral library digital file contains tables for the light properties of 20 materials, the output of the classification process will be 20 raster layers, and every pixel will be assigned a float value from 0 to 1. If the value is 0.5, that means that for the material elements designated for that raster layer, the material makes up 50% of the area in the geographically defined square pixel cell. With Tetracorder or similar algorithms, as the user inputs a smaller number elements, the process iterates through the DN values in the different band raster layers fewer times, and as a result of the developments made to the algorithm, it computes the likelihood for the presence of the inputted materials (on a scale of 0 to 1) with greater accuracy.

2.3 Classifying Minerals and Mine Operations with AVIRIS Data

AVIRIS data has also been used to map, in fine detail, the chemical properties as well as even soil types for broad geographic areas, such as an entire river delta after a period of intense flooding. Studies suggest that proportional mixtures of sand, silt, and clay, as well as mineral compositions within the soil, can be detected with a high degree of accuracy, based on a validation of AVIRIS classification against ground samples tested in a laboratory (Dutta 2015). Soil types can be precisely identified with the use of highly accurate classification methods such as the Tetracorder algorithm, along with hyperspectral imagery such as AVIRIS that is captured at more specific spectral band wavelength channels than other sensor platforms such as the spaceborne Landsat or ASTER image sensors. AVIRIS data is also collected at a finer spatial resolution (as little as 4 m pixel ground sample distance, depending on altitude of flight), which provides more a more distinct classification and a better estimate of proportional surface composition for each material (Rockwell 2005). Soil type can be precisely determined by detecting the presence of elements such as sulfur, magnesium, iron, and copper, and matching their proportional composition at a given point with known combinations for sand, silt, clay, and loam combinations thereof (see Figure 6). Laboratory spectral tests of different soil types reveal precisely what proportions of each base element is present, and these can be related to classification proportions returned by Tetracorder.

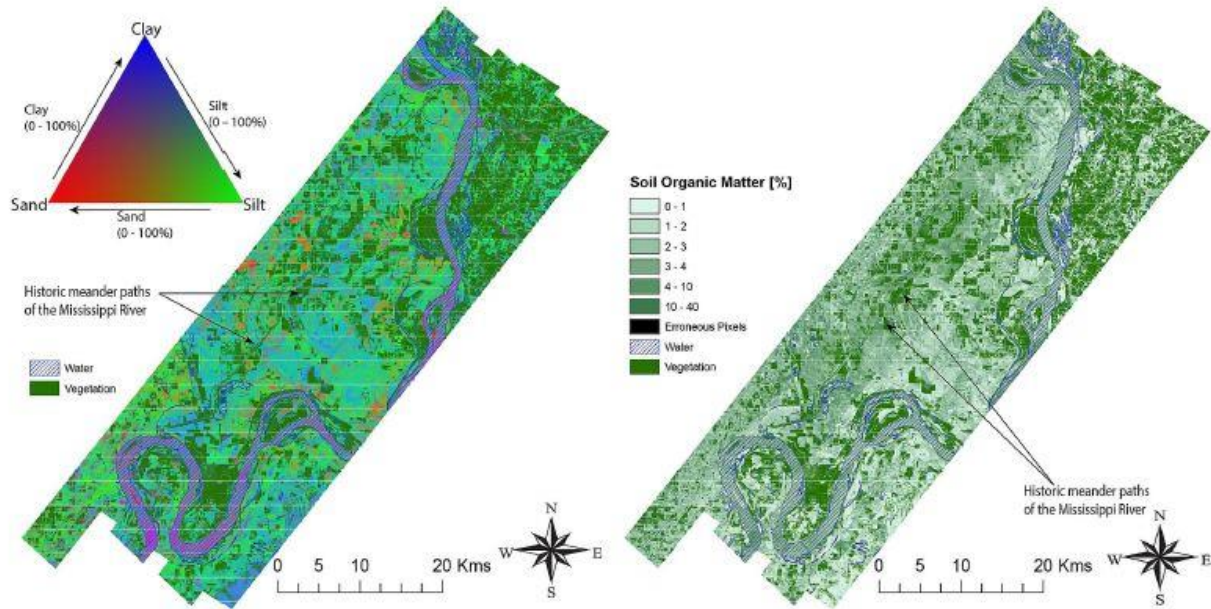


Figure 6 Soil composition classification displayed by type, along with vegetation, in the BPNM Floodway along the Mississippi River (left) and density of soil organic matter classified (right) from AVIRIS flight data (Dutta 2015)

Similar classification approaches using AVIRIS datasets with the Tetracorder and similar algorithms present an ideal approach to mapping the presence of minerals on the Earth's surface in areas in which large-scale surface mining operations are present. Just as chemical composition can be detected in soils to determine soil type using user-defined spectral parameters for each classification element, the presence of different mineral molecules on the Earth's surface, as shown in Figure 7. Minerals are made of molecular lattices that reflect and absorb light differently based on the specific atoms and molecules that make them up, and as a result the light reflected off of different minerals can be analyzed to accurately identify them. Spatially, images are divided into arrays of georeferenced cells, and spectrally, the cells making up an image show telltale reductions in band reflectance at wavelengths where a certain material absorbs light instead of reflecting it (Dalton 2007).

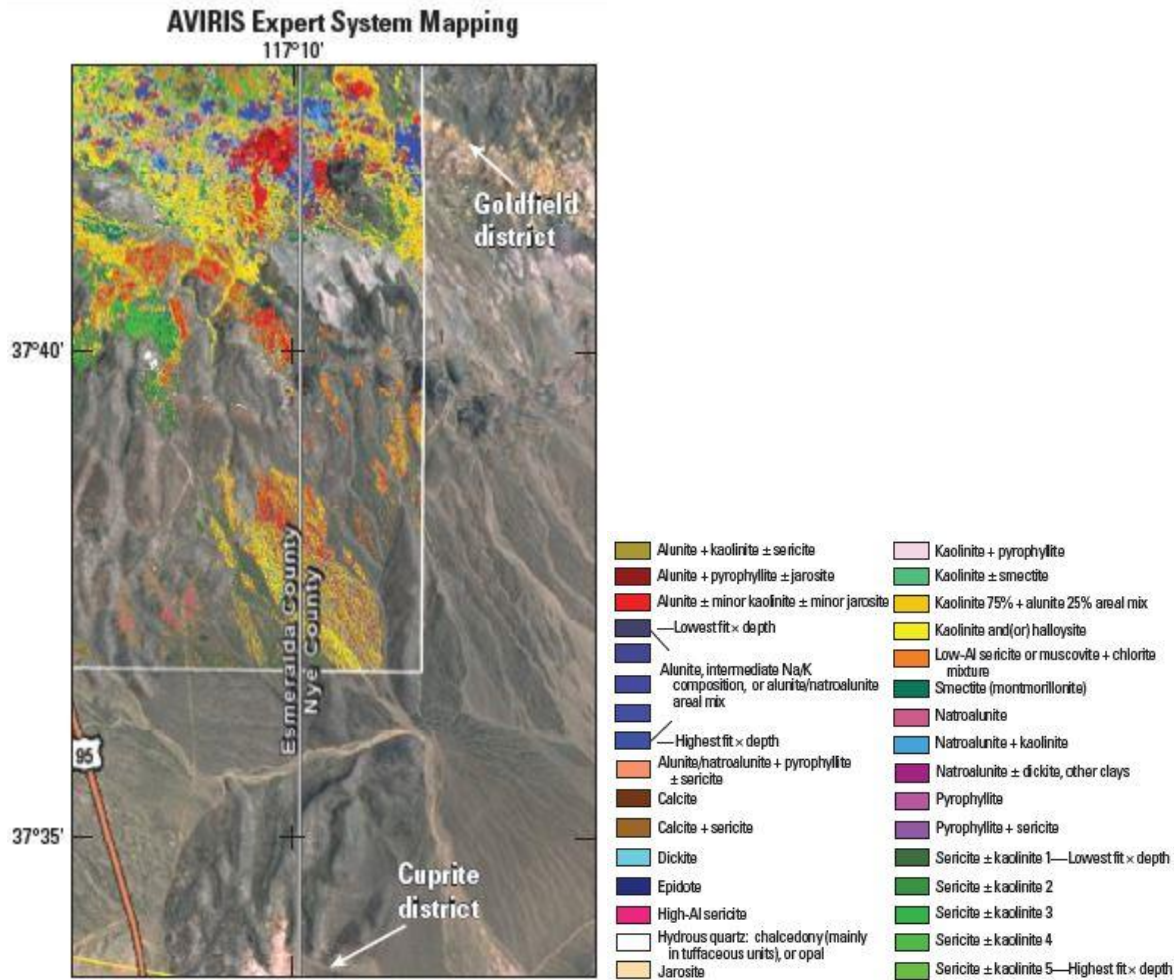


Figure 7 Surface mineral classification map for Goldfield mining district in Western Nevada (Rockwell 2012)

Classification algorithms can go a step further than merely identifying, mapping and analyzing surface composition of mineral elements to assess the impact of mining operations on the environment. Classifications of surface materials from AVIRIS data are combined with digital elevation models (DEMs) to analyze catchment from mine waste runoff by detecting precise material composition as well as drainage flow. This is possible when a small number of waste minerals are identified in a defined geographic region and used for classification purposes (Mars 2002). By converting output raster layers for classified mine waste minerals into a polygon feature class or as a simplified (reclassified) raster with defined integer values only, and

then inputting these areas into a flow analysis process with a DEM, the sources of these mine waste regions can be identified.

2.4 Impact of Legislation and Role of Spatial Data Analysis

The study area in West Virginia is unique in that it represents a region significantly impacted by two pieces of legislation: The Clean Water Act of 1972 and the Clean Air Act of 1963. Both pieces of legislation sought to protect at-risk populations near areas of dense industrial activity such as in West Virginia (Butler 1963). While these laws recognize the risks of mines and other industrial sites introducing toxic elements into the air and water networks that filter towards nearby populations, in areas such as southern West Virginia they have become far less effective in recent years. The Clean Air Act, for instance, specifically limited burning of sulfur-rich coal. However, the coal mined in the Appalachians has a lower sulfur content than the coal mined elsewhere, and an unintended consequence of the Clean Air Act was that surface mining operations in West Virginia expanded significantly (Hendryx 2016). Hilltop mining efforts that in practice are more likely to dump mineral pilings in neighboring valley and stream networks became more prevalent.

The Clean Water Act that sought to protect vulnerable downstream populations from such waste has been weakened significantly in the decades since its enactment. The 2005 Energy Act specifically exempted a variety of oil, gas and coal mining operations from protections that were previously in place (Lambert 2016). During this period, hilltop mining permits in West Virginia were issued at a greater pace than in any previous decade, according to permit data sourced from the federal Office of Surface Mining. Because of the expansion of these operations, and with only limited spatial data available for analysis, accurate image classifications can immediately serve to analyze the impact of these operations on neighboring populations.

Chapter 3 Methods

3.1 Data Preparation

The methodology for this study can broadly be categorized as consisting of three phases: Data Preparation, Classification, and Spatial Analysis. The Data Preparation phase pertains to the (3.1.1) *integration* of various spatial datasets directly required for this study, which includes the consolidation and conversion of these data, (3.1.2) implementation of thorough and sophisticated *quality control* measures to ensure accuracy of data and minimize error, and (3.1.3) the final *preparation* for these data into the software necessary to analyze the data effectively. Ensuring effective integration and quality of data is essential, if an accurate classification of materials within the raster dataset can be attempted.

The classification methodologies for this study involved classifying the AVIRIS data by two distinct approaches. The first was a supervised classification, in which vector polygon features representing a sampling of surface mine pilings were digitized and input as parameters for the classification algorithm. The returned layer represented areas matching the light properties of the points in those polygon feature areas. The second classification method was an automated approach, which was directed to identify areas containing significant amounts of Jarosite, Alunite, and Muscovite, ferric minerals typical of disturbed earth near surface mines. Both classification methods were judged in accuracy based on coincidence with verified vector data that represent precise mine locations in the study area (“ground truthing”). Data preparation encompasses all these processes and is vital to both classification and spatial analysis.

3.1.1. Data Integration

To successfully classify hyperspectral imagery and validate the respective classifications spatially, multiple georeferenced raster datasets were required, shown in Table 1. A

hyperspectral AVIRIS dataset with coverage throughout the study area and collected recently was sourced through NASA's JPL geoportal (http://aviris.jpl.nasa.gov/alt_locator/). AVIRIS data is collected aurally in a push broom swath, which images the ground underneath the airplane with a variable width dependent on the lens focal length and the altitude flown. For the study area examined in this research, a single swath dataset provided coverage, as the study area was tailored to the availability of hyperspectral data that coincided with areas of heavy mining. Multiple swaths can be mosaicked together to examine a larger area if necessary, with an identical methodology employed prior to merging the raster datasets. AVIRIS data packages contain multiple files and extensions, to include a DEM as well as an orthorectified imagery dataset that is presented in a binary format. The data for each pixel includes the latitude, longitude, and 16-bit integer value associated with each of the 224 wavelength bands that are layered in the image file. These band layers can be unpacked into separate datasets for processing. They can also be integrated as a single binary file into a GIS such as Esri ArcMap with no conversion necessary and manipulated through the layer's display properties. In this study, band combinations were selected specifically to ensure data quality and that the presence of clouds was minimal. The band combination of 36 (centered at 657 nm), 19 (centered at 550 nm), and 9 (centered at 482 nm) as red, green, and blue, respectively, represented the *natural view* for the image dataset. The natural view represented how the scene appeared to the naked human eye in the visible spectrum of light.

<i>Spatial Data</i>	<i>Source</i>	<i>Name</i>	<i>Data Type</i>	<i>Creation Date</i>	<i>Scale/Spatial Resolution</i>	<i>Size on Disk</i>
AVIRIS Image Cube	NASA JPL	f090714t01p00r12	Binary File	Jul 2009	16.2m	5.8 Gb
NAIP Orthoimagery	USGS	3708002-3708145	Jpeg 2000	Oct/Nov 2010	1m	2.7 Gb
Mine Locations	OSM eAMLIS	WV_AOI_SurfaceMines	Shapefile	2010	1:24,000	6.7 Mb

Table 1 Data requirements

Fine-resolution orthoimagery was used to verify the data relating to surface mines and mining operations. It was also used to create vectors at larger scales for application in the supervised classification. *Fine resolution* refers to remotely sensed imagery that represents a ground sampled distance small enough that individual features such as buildings, roads and industrial sites can be easily identified (typically less than three meters). The National Agriculture Imagery Program (NAIP) aerially collected orthoimagery was sourced through the United States Geological Survey (USGS) geoportal (<http://earthexplorer.usgs.gov>). The imagery is collected at a 1 meter spatial resolution, which allows for a detailed examination of the surface, while encompassing the entire study area. The NAIP imagery used in this study was collected from October- November, 2010, and, therefore, represents the same terrain at a similar temporal resolution as the AVIRIS dataset used for classification.

Vector data in the form of a merged point feature class was also required to identify both active and inactive surface mines in the study area. These data were vital to validating the results of the study classifications. They served as a “ground truth” reference in this regard. The mining feature data were sourced from the OSM eAMLIS service. Data is current as of 2009 and was created at a 1:24,000 scale. The point feature class represents both inactive and active surface mines, and includes coal mines as well as mineral mines (such as copper). Inactive mines were

included in this study because of the signature that they leave behind, e.g., large mounds of disturbed earth near the mine site, typically in valleys adjacent to the hilltops on which surface mines tend to operate.

3.1.2. Data Quality

Data quality protocols must be enforced for both the raster and vector datasets integrated for this study. For both classes of raster data, the hyperspectral AVIRIS data as well as the aerial orthoimagery, precise horizontal (XY) positional accuracy needed to be verified to a designated standard. The orthorectification, alignment, and mosaic processes were completed by the agencies that collected and produced these datasets (NASA's JPL and the NAIP, respectively). For this study, it was crucial to gauge the effectiveness of the orthorectification by checking both datasets against a known standard. In this case, the Continually Operating Reference Station (CORS) site located in the study area and operated by the National Geodetic Survey (NGS), was used to confirm the horizontal position of the raster layers used in the project. A tolerance of 1 pixel per dataset was allowed, which represented less than 16-meter horizontal accuracy for the AVIRIS data and 1 meter horizontal accuracy for the NAIP dataset.

Validating the mine feature class data was paramount to the accuracy and error assessment for the classification efforts. While both active and inactive surface mine points appeared to be accurate in terms of the presence of distinguishing characteristics in the vicinity, a number of inactive mines had vegetation growing over the surface of the earthen mounds nearby. These were included in the study for the purposes of testing the accuracy of the classification. This assumed that the mines were active within 11 years of the date of collection for the hyperspectral image dataset (from 2000 to 2011). Figure 8 displays three of the large-scale

surface mines located in the study area and verified with the NAIP orthoimagery that was collected at the same time as the AVIRIS dataset.

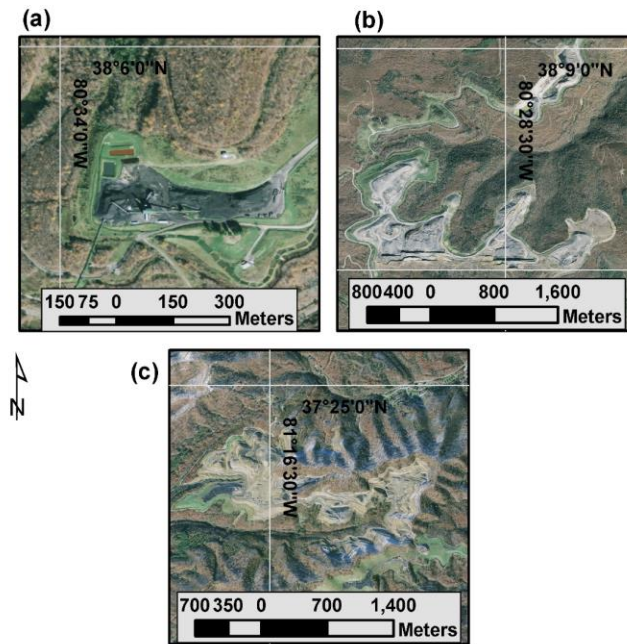


Figure 8 An example of three different surface mines identified from the OSM feature class verified in NAIP imagery (doi Oct/Nov 2010).

3.1.3. Data Preparation

The first step of preparing the hyperspectral imagery dataset for classification was to integrate it into IDRISI TerrSet. AVIRIS data derived from the JPL file transfer protocol (FTP) site are compressed in .tar format. They require extraction before they can be imported into IDRISI using the Geospatial Data Abstraction Library (GDAL) Conversion Utility within TerrSet. The GDAL import process input the orthorectified image dataset (a single binary file after the compressed .tar folder is unpacked) and output 224 raster files in IDRISI's native .rst format. These files each represent a different band of the electromagnetic spectrum, from approximately 365 nm wavelength at the center of the first band to 2496 nm wavelength at the center of the 224th band. Each raster layer produced in the .rst format therefore represents approximately ten nanometers of light wavelength, and within each channel represents a single

16-bit luminance value for each geographically referenced 16.2-meter-wide pixel cell. A small number (<1%) of pixels contain null values in the AVIRIS dataset used in the study. These occur predominantly at the edges of the raster layer where these null values default to a 16-bit value of -9999 on import to IDRISI it was important to set these values to 0 (the minimum luminance value for all pixels) in order to stretch the light values more effectively and leading to a more effective classification.

The stretch function accentuates the data in each raster dataset by removing DN values outside of a statistical majority of reflectance values present in a layer. The function narrows the range of DN values and therefore creates greater variation in the presented pixels. For this study, properly identifying the mean DN value and standard deviation from this mean were crucial to stretching the respective band layers to increase the effectiveness of the classification. The bands were grouped into a raster group file (.rgf) and numeric histograms were computed for the group. Means and standard deviations returned by the histograms were then used as parameters for stretch functions applied to each band, one by one.

The stretched AVIRIS hyperspectral imagery bands were then re-grouped and processed through IDRISI's screen function. The screen function detects the presence of atmospheric distortion by analyzing the spatial correlation of light values across an entire spectral band of imagery. Pixel variation outside of the normalized (0 to 1) scale of .6 as a lower threshold and .99 on the upper threshold indicated a high degree of atmospheric scattering. While atmospheric scattering of light is a topic outside of the scope of this study, for a more effective classification, it was necessary to identify bands that do not provide clarity and strong dynamic range. The screen function was processed in this study on the raster group containing the stretched AVIRIS

band layers, removing any bands that presented an unacceptable degree of atmospheric scattering.

Two distinct classifications – supervised and unsupervised - were performed in this study. The supervised classification required polygon vector training sites as an input to represent the surface material that the classification sought to identify. The supervised classification served as a controlled test of hyperspectral image classification for surface mining operations in this study, while the unsupervised classification (based on a digital spectral library) served as the primary focus of the efficacy for automated identification of surface materials in a GIS. Given the broader dynamic range and extremely stratified hyperspectral dataset used in this study, fewer *training sites* or polygon features representing singular surface materials were deemed to be necessary. These training sites were digitized within the earthen mounds near fourteen of the identified larger-scale surface mines in the training area, using the natural view color composite from the AVIRIS dataset as a guide, and ensuring avoidance of non-mineral materials such as roads, vegetation, and man-made materials such as buildings and construction equipment. These polygon features were saved in a .vct format native to IDRISI, and all were created with attribute values of “1”, indicating identical surface composition for the supervised classification module.

The AVIRIS image group was also classified with data from pre-loaded spectral libraries. These libraries (managed by the JPL as well as the USGS) are available for order and can be imported into IDRISI. In order to perform a more targeted classification, the minerals classified were limited to Jarosite ($\text{KFe}^{3+}_3(\text{OH})_6(\text{SO}_4)_2$), Alunite ($\text{KAl}_3(\text{SO}_4)_2(\text{OH})_6$), and Muscovite ($\text{KAl}_2(\text{AlSi}_3\text{O}_{10})(\text{F},\text{OH})_2$). To precisely identify these specific sulfates, the light reflectance and absorption features (representing each mineral’s specific spectral profile) were loaded as a

hyperspectral signature file into IDRISI, after which the two signature files were combined into a single hyperspectral signature group (.hgf extension in IDRISI) for the purpose of classification.

3.2 Classification

Two classifications for the AVIRIS dataset were conducted using the same *hyperabsorb* function in TerrSet. This function inputs a hyperspectral signature group (either trained from a vector polygon layer or collected from a spectral library) and is then processed in conjunction with the image group. The image groups were first classified with the training sites in a supervised classification, and then were classified with the minerals of Jarosite and Alunite loaded from the spectral library. The *hyperabsorb* function processes all image band layers within the image group at every pixel in the image dataset. For each pixel, a likelihood of classification is returned in the form a “fitting” and a “depth” layer. Fitting is presented as a fraction, such that if the value returned is equal to 1, that pixel entirely represents the given mineral or material indicated in the classification. While this value might rarely equal 1 for an AVIRIS pixel measuring 16 meters across, a value over .5 might indicate a strong presence of the indicated material. The depth layer is processed automatically as well by the *hyperabsorb* function, thereby reducing noise throughout the scene to more clearly identify the classified surface materials.

The result of the hyperspectral classification processes were two sets of layers: (1) fitting and (2) depth - both scaled as likelihood fractions from zero to one. The *overlay* function takes these ratios a step further through visually combining them into a single raster overlay. This is done by dividing every pixel’s DN value in the fitting layer for each mineral by the DN value in the depth layer from the corresponding pixel in the depth layer. This “maximum support classification” step incorporates both factors of *abundance* of spectral similarity for a given

mineral, as well as the similarities in the *depth* areas representing absorption areas in the spectral curve. These two principles are represented by the fitting and depth layers, where the division of depth into fitting provides a single layer output representing the overall ratio (for each individual pixel represented in the study area) for the presence of the classified material. This is done for the target minerals as well as for the surfaces matching the areas digitized near mining operations, for the unsupervised and supervised classifications, respectively.

For the automated classification, it was necessary to remove extraneous surfaces that might be identified as similar to the mineral elements targeted, but that might not intersect with surface mines. The reason for this extraneous classification is discussed in detail in the results chapter, but for the methodology it was vital to identify areas of concrete as well as water, as these surface materials were commonly identified as containing ferric mineral elements. The same automated classification used to identify the mineral elements targeted in this study was used to classify concrete and water, thereby creating binary raster layers representing both materials. To obtain the spectral signatures required for the *hyperabsorb* function as inputs, the *hyperautosig* function targeted 33 different classes of surface materials in the entire study area represented in the AVIRIS hyperspectral imagery. The hypothesis that proved correct was that the output – 33 different raster layers each representing an automatically distinguished spectral curve – could be analyzed over fine-resolution orthoimagery. The second output of the *hyperautosig* function were the spectral curves corresponding to the output classification layers. Once the specific output raster layers representing concrete and water were identified, their corresponding hyperspectral signature files were input into the *hyperabsorb* function to more effectively classify these materials. This insured that these areas could be removed by raster calculation from the automated mineral classification.

For each of the two output layers representing the returns of the supervised and unsupervised hyperspectral classifications, the *reclassify* function was performed to identify areas where the queried minerals are most concentrated on the surface. Pixel values for these final classification layers were values from 0 to 1, representing anywhere from no trace of the minerals to a strong concentration. The “likelihood” reclassification for each mineral - Jarosite, Alunite, and Muscovite - was 0.3 and above for each mineral element.

These binary rasters were then added together by raster calculation, and any value above 0 was reclassified again to 1. The reasoning here was that for the final output, the strong presence of any of these minerals was deemed a positive indicator for the presence of a surface mine. Once combined and reclassified, the data was then cleaned by removing (via raster calculation) the binary rasters representing concrete and water.

3.3 Spatial Analysis

To effectively measure the accuracy of both classification approaches, the final classification layers were converted from raster to polygon in ArcMap. These resulting classification layers may still have noise present in the form of loose pixels that converted to a polygon feature class and were represented as small squares. To eliminate these erroneous pixels, the Spatial Analyst toolset was utilized to calculate the area for each feature in the two polygon feature class layers. All features smaller than 400 square meters with a value of 1 (meaning lower concentration of minerals) were queried and deleted, and all features that were smaller than 200 square meters with a value of 2 (meaning higher concentration of minerals) were queried and deleted. As a final measure to clean the output polygons, the *smooth* function was applied to each feature class with a tolerance of 32 meters (about two pixels from the input hyperspectral raster) utilizing the Polynomial Approximation with Exponential Kernel (PAEK)

Algorithm. While the final output raster is represented as rows and columns of square values, the real-world features they represent are not. In the final classifications, the pixels represent proportionality of the presence for the targeted minerals. Therefore, a smoothed area more accurately reflects the irregularly shaped earthen mounds typical of surface mines. A thorough analysis of the outputs of the smoothing algorithm confirmed that the results of this function more accurately represented the real-world features.

An iterative search was performed through each mine location indicated in the final export of the prepared OSM shapefile. For each mine location, the two classification methods were tested as to their respective ability to detect mineral elements within a buffered distance of 500 meters from that mine location, using the *buffer* and *intersect* functions found in ArcGIS. Further, to quantify and effectively establish the ratio of false returns to accurate mine sites, an optimized hot spot clustering function was performed on each final feature class (automated and supervised). Clusters (established by counting incidents within a fishnet polygon) were grouped as features, to distinguish individual mine locations. These clusters were then analyzed and counted, with clusters greater than 1,500 meters from any known mine location deemed a false return.

Chapter 4 Results

The automated hyperspectral classification tailored specifically for the purpose of identifying surface mines proved to be accurate, with a correct identification of 51 out of 52 (98%) known surface mines in the study area. The “known surface mines” include mines that had been active at any point during the eleven years prior to the hyperspectral image collection date. This means that the automated mapping approach is able to identify older mines as well, which is especially important for environmental applications as large-scale surface mines can pose a substantial ecological risk for decades after closure. Furthermore, the automated classification identified in its output polygon feature class many possible surface mines that actually represented abandoned mines that had been inactive for eleven years or more prior to the image collection date. This further indicates the effectiveness of the classification methodology as a tool not just in monitoring industry, but in organizing cleanup efforts and waste control measures in other areas with heavy mining.

The supervised classification proved accurate as well, identifying 50 out of 52 (96%) known surface mines in the area. While the supervised classification identified and mapped these features with high accuracy, there was a greater amount of “noise” or false returns present in the output polygon feature class. The supervised classification approach’s high degree of accuracy was expected, given the extensive user input in preparing an input polygon shapefile that represented sample surface mine pilings from around the study area. The presence of noise and the reliability of the primary automated methodology used in this study will be discussed later in this chapter. The mapped outputs from both the automated and supervised classifications for a subset of the study area are shown below in Figures 9 and 10, respectively.

Central Study Area Mine Classification Results

SCALE 1:150,000

Coordinate System: UTM Zone 17N
 Datum: North American Datum 1983
 Imagery: Landsat ETM+
 Date of Image: May 2002
 Elevation Data: SRTM Relief
 Units: Meters

Legend

- Inactive Mine
- Surface Mine Active 2000-2011
- 500m Buffer from Active Mine
- Study Area
- Automated Surface Mine Classification

Active Surface Mines:	52
Identified in Automated Classification:	51
Identified in Supervised Classification:	50

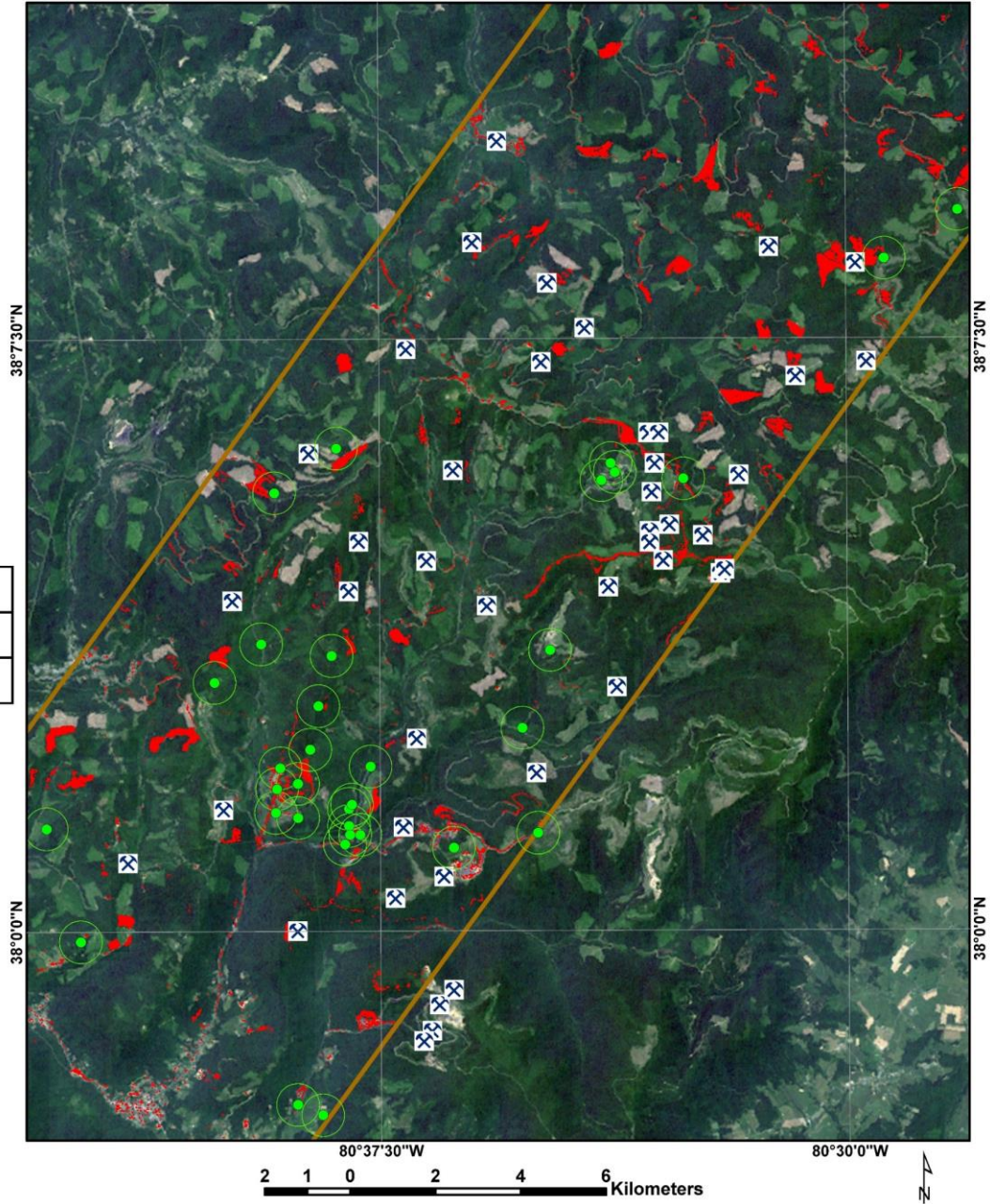


Figure 9 Automated classification returns overlaid on Landsat ETM+ imagery, with both active and inactive mines represented, and 500 meter buffer from active mines.

Central Study Area Mine Classification Results

SCALE 1:150,000

Coordinate System: UTM Zone 17N
 Datum: North American Datum 1983
 Imagery: Landsat ETM+
 Date of Image: May 2002
 Elevation Data: SRTM Relief
 Units: Meters

Legend

-  Inactive Mine
-  Surface Mine Active 2000-2011
-  500m Buffer from Active Mine
-  Study Area
-  Supervised Surface Mine Classification

Active Surface Mines:	52
Identified in Automated Classification:	51
Identified in Supervised Classification:	50

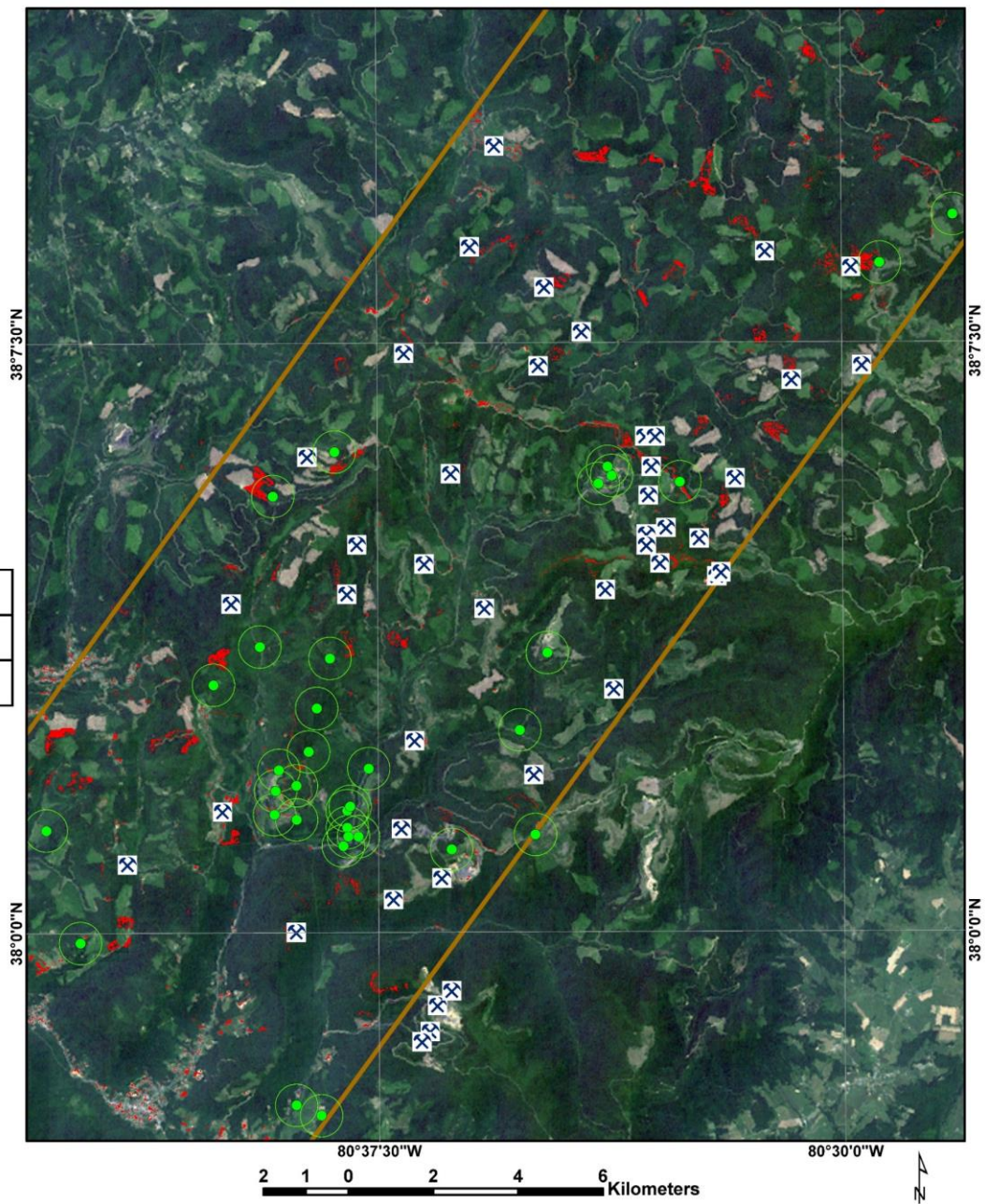


Figure 10 Supervised classification returns overlaid on Landsat ETM+ imagery, with both active and inactive mines represented, and 500 meter buffer from active mines.

4.1 Data Quality Inspections

The quality and accuracy of this study depend strongly on the quality of the input AVIRIS hyperspectral image dataset. With a significant reliance on the quality of a single dataset, a thorough inspection of quality was necessary to ensure the reliability of the results and output spatial data. The horizontal accuracy of the imagery, presence of noise in the raster bands, atmospheric distortion that might be present in the imagery, and the presence of noise that relates specifically to the elements distinguished in the automatic classification all present a serious risk to the potential effectiveness of the algorithm being tested in this study. If present in the data above a pre-determined tolerance level, these quality elements could bring any classification or map output produced by the study into question.

4.1.1. Horizontal Accuracy

Verifying – and, if necessary, correcting the horizontal accuracy of both the AVIRIS hyperspectral imagery and the NAIP orthoimagery was essential to establish an effective return of the two different classification algorithms, and towards confirming the accuracy of those returns. Both datasets were orthorectified and georeferenced in the coordinate system of UTM Zone 17N, with the ellipsoid and datum of the World Geodetic System (WGS) 1984. A number of advantages exist towards utilizing image datasets that were created using the same geographic reference system. First and foremost, any reprojection that might have been required could significantly alter the data. For the AVIRIS data especially, where each pixel in each of 224 bands represents a 16-bit integer value, a reprojection would have meant possibly altering those values directly. This can occur even with a nearest neighbor resampling of raster data layers. The reason that an alteration takes place is that pixels, by definition, represent a small square area on the Earth's surface. An area referenced in a geographic coordinate system will be tilted when

compared or changed to a UTM-based reference system, and correcting or changing this tilt necessitates using *fractions* of pixels. As splitting a pixel is impossible, reprojection and resampling algorithms will either use the value of that pixel's *nearest neighbor*, or directly change the value by averaging the neighbor values, depending on which algorithm is utilized. Another clear advantage to having both image datasets projected and rectified in the WGS84 UTM coordinate system was that the units for this coordinate reference system (CRS) is meters, which means that pixel mensuration is made significantly easier.

The accuracy of the NAIP dataset was measured against the single Continually Operating Reference Station (CORS) situated within the study area (in Elkins, West Virginia). CORS stations are operated by the National Geodetic Survey (NGS) and provide extremely precise, sub-centimeter positions at fixed sites that continuously update their position, in this case every second. The site at Elkins, with the site identification WVNR, is identified by the photographs in Figure 11, and by the precise position 38 53 44.50553, (N) 079 51 30.26994, (W) with the North American Datum (NAD) 1983 reference system.



Figure 11 Views of GPS reference station in Elkins, West Virginia (Image Source: <https://www.ngs.noaa.gov/CORS/>)

Converting this single point to the WGS84 UTM Zone 17N CRS, it is measured within the NAIP image dataset directly to identify any possible misalignment. In Figure 12, this position is indicated in the imagery. While a single reference point cannot speak to the alignment and horizontal accuracy of a relatively large orthomosaic dataset, for the purpose of this study, it serves to identify any potential shift present in the data.



Figure 12 CORS precise coordinates represented as point over NAIP imagery

The NAIP image dataset is accurate to within 5 meters, which, for the purposes of this study, is ideal. The secondary accuracy measurement is for the AVIRIS dataset used in the study. An alignment of less than one pixel from the AVIRIS data with a coarser 16.2 meter spatial resolution to the NAIP data is essential for two reasons: (1) so that the polygon feature class representing surface mine pilings digitized with the NAIP data as a reference matches the

AVIRIS dataset for which it serves as input in the supervised classification; and (2) to confirm that the hyperspectral imagery accurately reflects the corresponding positions on the Earth's surface. This latter point is especially important in applications of the automated classifications conducted after this study is complete. Were the data to be misaligned or shifted from known reference points, even an accurate classification would not properly identify surface mines in terms of positional accuracy.

Twelve readily identifiable reference points measured the difference in horizontal position between the AVIRIS hyperspectral dataset and the NAIP data. These reference points, shown in Table 1, were evenly distributed throughout the study area, and corresponded to durable man-made construction materials with low or no height above ground level. All twelve reference points, identified in the AVIRIS natural view color composite, fell within one half pixel (about 8 meters) of the corresponding point in the NAIP dataset. This test for horizontal accuracy proved that the datasets were orthorectified and projected accurately, and that further data quality tests could continue prior to classification.







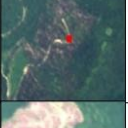

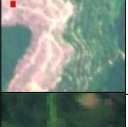





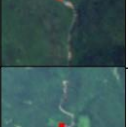

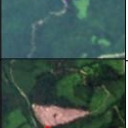

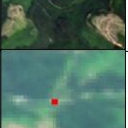





ID	Easting	Northing	Description	AVIRIS Image	NAIP Image
1	598650	4305530	Corner of Runway		
2	597071	4297430	Corner of Industrial Yard		
3	589798	4286240	Intersection of Cropland		
4	582938	4284134	Corner Bend in Road		
5	574993	4280639	Corner Roadway on Mine		
6	576921	4265871	Roadway Crossing		
7	562080	4258310	Road Clearing		
8	551469	4236327	Corner Bend in Road		
9	540207	4228702	Corner Bend in Road		
10	541131	4218231	Edge of Mineral Piling		
11	525034	4211237	Roadway Crossing		
12	524226	4195157	Corner of Parking Lot		

Table 2 AVIRIS dataset horizontal accuracy assessment

4.1.2. Atmospheric Distortion

The presence of atmospheric distortion would diminish or entirely alter any returned output spatial data from either classification approach. The effectiveness of the automated classification methodology, which is the primary focus of this study, cannot be determined without clarity of data. Atmospheric distortion (or *scattering*) would not only diminish the returns of the classification, but could alter the light to the extent that surface materials cannot be identified correctly (or might be completely misidentified) from the algorithm performed with the hyperspectral raster bands. For this reason, this study and similar experiments can and should only be attempted with data free from significant atmospheric distortion.

The methodology tailored from background research indicates an upper limit for *autocorrelation* of .99 and lower limit of .6. This represents a clear and reliable image band. In the Idrisi TerrSet *screen* module, this autocorrelation range was applied to each of 224 bands in the hyperspectral dataset. All bands fell well within this range, as indicated in the autocorrelation curve represented in Figure 13. While this analysis confirming clarity of data corresponds with the fact that in the natural view imagery, very few clouds and almost no haze is apparent, there are instances where apparently clear data might have invisible particulate matter that might skew the results. Such distortion would appear in the autocorrelation analysis.



Figure 13 Autocorrelation Analysis in *Screen* function for 224 bands in AVIRIS dataset

4.2 Results of Classification

The automated classification returned a highly accurate polygon feature class coinciding with 51 of 52 surface mines in the study area. The returned raster output layers for the automated classification of Jarosite and Alunite represented extremely limited coverage in the study area, at any classified value. Interestingly, for the overwhelming majority of the study area, these minerals went undetected, despite background research indicating that such minerals might be prevalent in mineral pilings near surface mines in terrain such as that studied in this analysis. Despite these limited returns, in keeping with the methodology and to rigorously test the algorithm, these classification raster layers were added by raster calculation to the Muscovite layer, which provided ample returns and seemed to highlight surface mines with greater percentages (over 0.25 on a normalized scale of 0 to 1) for the output fitting layer. In Figure 14 (a), this raw output raster layer is represented in greyscale, with areas measured as having a greater fitness for the presence of Muscovite (as determined by a correlation with the hyperspectral imagery and the manually entered spectral properties for the mineral) are represented in white. In the binary raster reclassified in Figure 14 (b), Muscovite values over the level of 0.25 are shown in green, with all else shown in black. This binary raster has not been combined with the Alunite and Jarosite binaries, and has not been processed to account for and remove concrete and water values.

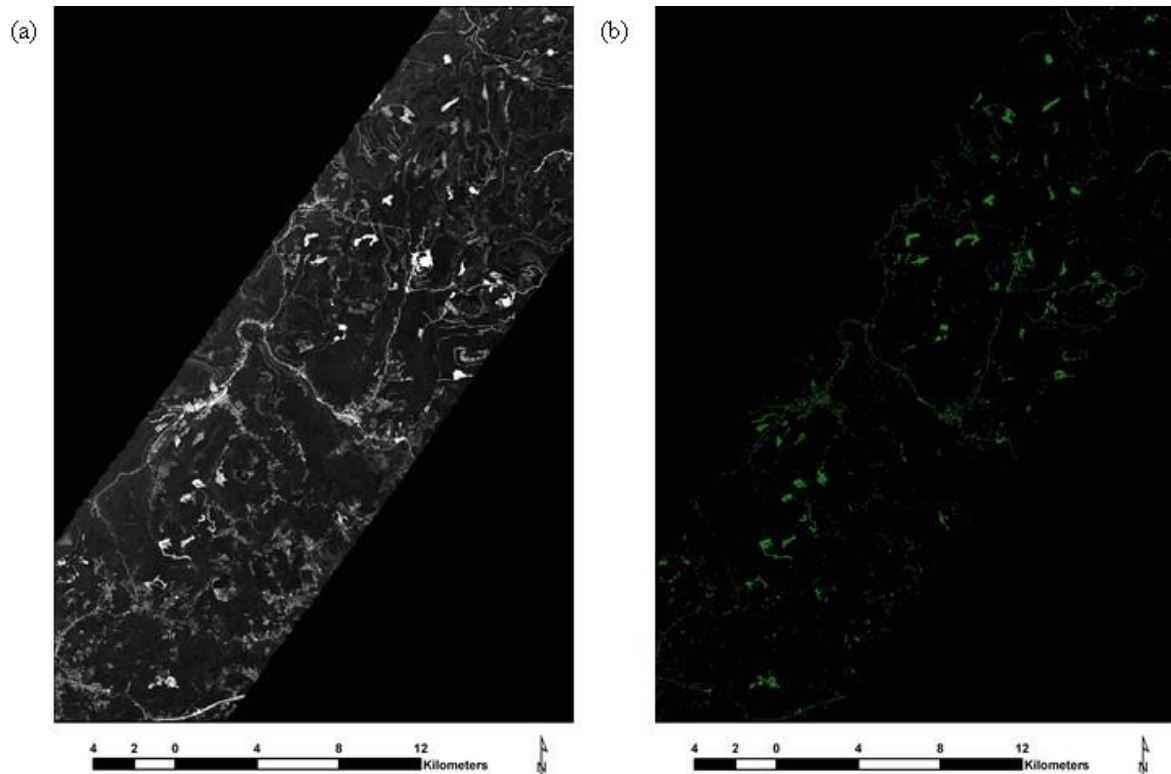


Figure 14 (a) Raw output of Muscovite *Hyperabsorb* automatic classification, and (b) reclassified (binary raster) Muscovite automatic classification

The classified layers representing concrete and water did not coincide with the surface mines in any part of the study area. This exclusion, and the apparent accuracy of this sub-classification also performed automatically using a spectral signature developed in testing, mitigated what could have been a major error with the automated classification methodology. Had the water and concrete classifications also returned erroneous or partial areas in or around the surface mines, these areas would have been removed from the true mineral classification (again, by raster calculation), and the automated approach would have returned fewer surface mines in the final vectorized output. The very reason that the concrete and water classifications are needed to be subtracted from the output is not a false return, but the presence of these minerals in hard construction materials as well as drainage networks throughout the area. While

the presence of mineral elements in concrete and buildings is sensible, their presence in large traces throughout river networks speaks to the heart of the issue, that these surface mines pose a grave environmental threat to the greater area (in some cases many miles away from the site and for decades after their closure).

An example of the output for the automated classification approach is shown in Figure 15. To the right, the classification polygon feature class is draped over a rendered 3D model of an area of dense concentration of surface mines in the central study area. The model is rendered with the NAIP orthoimagery draped over ASTER Global DEM elevation data, with no vertical exaggeration represented. In the image, one large active mine and one small active mine to the top and right of the image (respectively) are visible, along with an inactive mine to the left of the image. All three were classified as such in the output layer.



Figure 15 Output polygon feature class from automated surface mine classification, draped over 3D model

While the supervised classification performed similarly well with a rate of 50 out of 52 surface mines identified, the vectorized final layer represented much more than just the surface mines themselves. The automated classification approach was able to filter non-mineral results much better than the control, which, in this study, was the supervised classification. The

supervised approach utilized a more common methodology of creating *training sites* or polygon vector feature data representing examples of what the classification is targeting (e.g. pilings near these mines). The method bears repeating in the results discussion because this is the reason behind the returned coverage in the output feature class. Not all of the earthen pilings around these mines have the same material composition, and the classification algorithm does not seek form or shape, but spectrally similar components. Therefore, the mixture of normal, healthy soil, vegetation, and various miscellaneous minerals and materials in these pilings that may or may not be hazardous are mapped by the algorithm in the rest of the study area. While the supervised classification was able to accurately identify mines throughout the area at a rate of 96.2%, it also misidentified scattered polygons throughout the region.

Both classification approaches provided extremely similar results in the vicinity around larger mines, and especially mines that were operating at the time the hyperspectral imagery was collected. This similarity is especially surprising given the difference in the approaches and algorithms used by each method, as well as the need for substantial user input on the part of the supervised classification. The results of the automated and supervised classification outputs are overlaid on fine-resolution orthoimagery for a sample mine in the study area in Figures 16 and 17, respectively. As with all the larger mines, both classifications are able to effectively map the larger earthen piles and exposed regions around the mine itself. The fine resolution orthoimagery in these examples has a 1 meter spatial resolution for ground sampled distance, and features are clearly identifiable within the raster dataset.

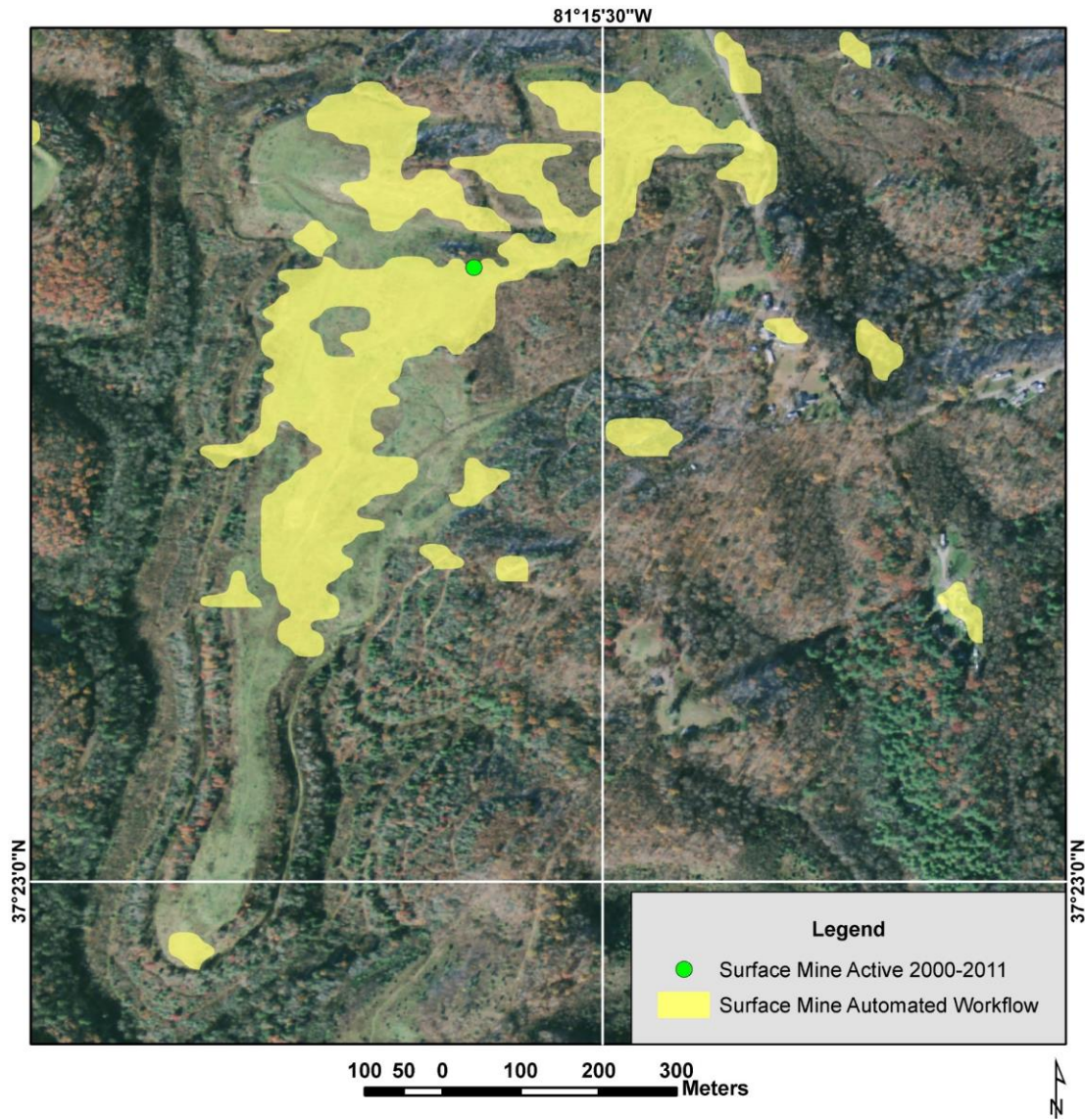


Figure 16 Results of automated surface mine classification, overlaid on NAIP orthoimagery

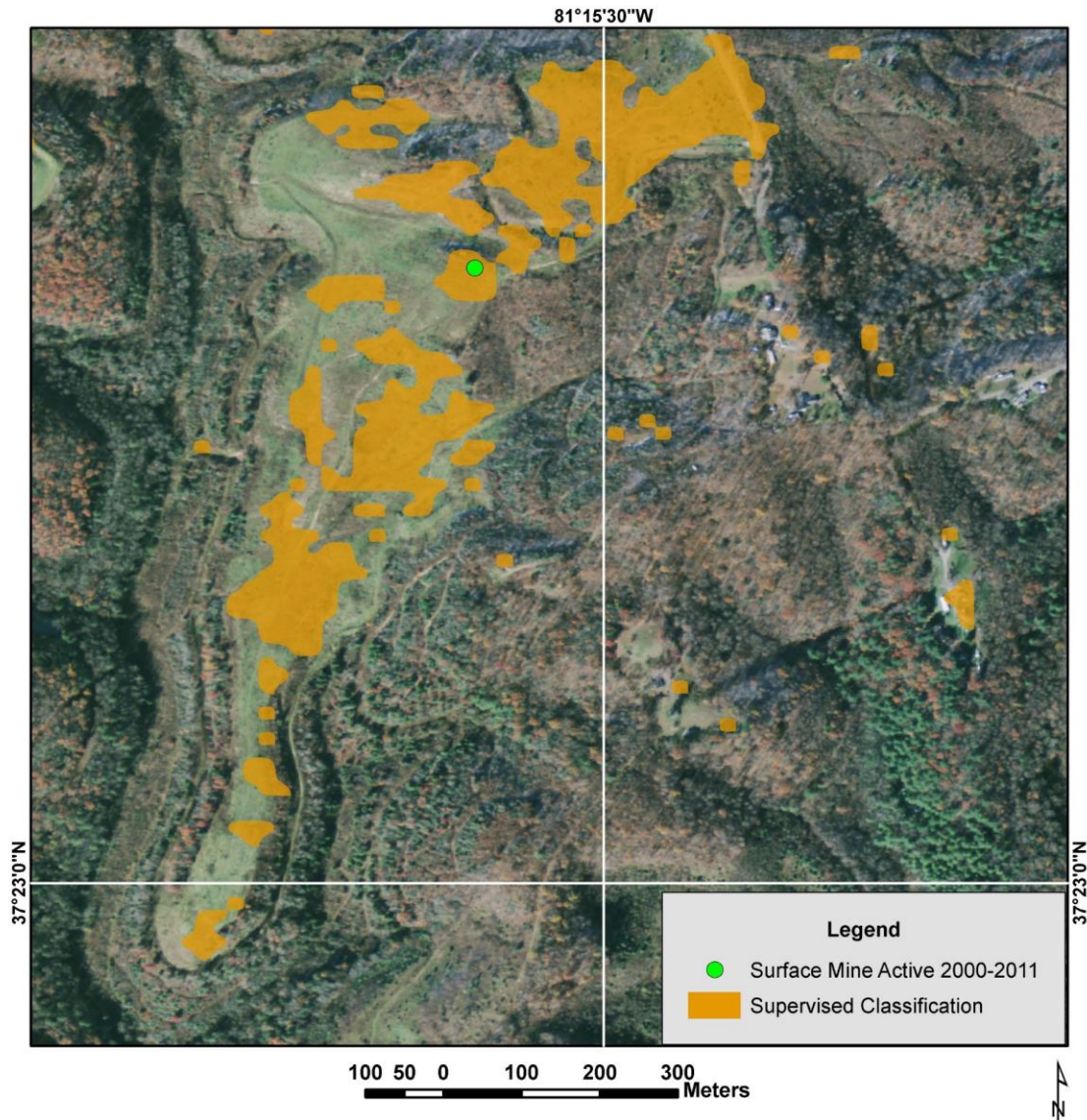


Figure 17 Results of supervised classification of surface mine, overlaid on NAIP orthoimagery

While the “false returns” or fragmented features away from surface mines were more prevalent in the supervised classification results, they were still present in the final output of the automated classification approach. These smaller features in the polygon feature class tended to represent concrete as well as the banks of rivers. The reason for the inclusion of these areas in the classification output are simply that these surfaces do contain one of the minerals being

targeted in the automated classification, but were not removed with the other areas classified as concrete or water. With the “cleaning” or removal by raster calculation of the areas classified as water, the banks of the rivers themselves where these minerals are deposited would not be removed because they are not water. Fragments of the concrete areas remain in the output because the concrete classification is not all-inclusive. Rather, as it is a diverse mixture that can come from a variety of material components. An example of such “false returns” is shown in Figure 18.

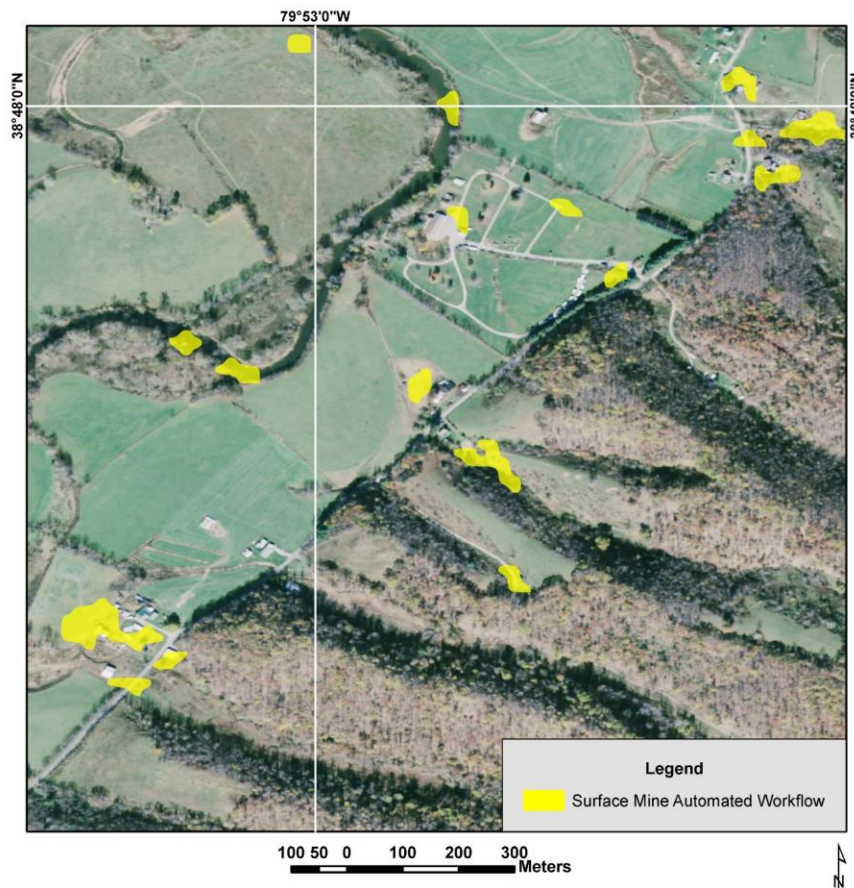


Figure 18 “False returns” in automated surface mine classification

Chapter 5 Discussion

The results of this project provide more than merely a validation of the methodology being tested, shown in Table 3. The primary measure of accuracy in this study is the intersection of classified surface mines in the output spatial dataset and real-world surface mines identified in detail by the OSM feature data. In this measure, both the automated and supervised classification methods proved effective. However, significant focus was placed on the *likelihood* of the classification correctly representing a surface mine site. This latter measure assessed the ratio of false returns to correct ones, and in this measure the automated classification proved significantly more accurate than the supervised classification. The automated classification had a false return rate of 37.3% - significantly lower than the rate for the supervised classification, 84.7%.

	Number of Active Surface Mines	Number of Surface Mines Intersecting Classification (500m buffer)	Number of Classified "Clusters" of Surface Mine Pillings	Number of Classified "Clusters" Intersecting Known Mines	False Return Percentage	Accuracy of "Cluster" in Mapping Known Mines (1500m)	Accuracy Percentage (Mapping Known Mines)
Automated Classification	52	51	67	42	37.3%	62.7%	98.1%
Supervised Classification	52	50	85	13	84.7%	15.3%	96.2%

Table 3 Results of classifications and false return rates

The implications of an efficacious automated classification approach that can be used to map mining operations without substantial analyst input are substantial. While hyperspectral imaging sensors and airborne collection operations remain prohibitively expensive, it is

important to develop and identify valuable practical applications in order to encourage development and adoption. Mapping surface mines is but a single possible application. Further research into both similar, environmentally-oriented applications as well as commercial and defense mapping applications are necessary to emphasize the clear value of and potential in this technology (Steinitz 2016). Further research is also necessary to better understand how this approach to mapping and classification with hyperspectral imagery might function in different types of terrain and environments around the world.

Mapping the areas of potentially hazardous elements around surface mines can significantly impact practical planning and informational processes carried out to manage larger populations and administrative areas. An estimated 33,142 people out of a total 47,705 people residing within the study area live downstream from surface mine locations (based on a spatial analysis of the mine data as well as hydrology networks and digital elevation data). Identifying specific impacts to downstream populations from the classified surface mines is just one example of how this study can influence such administration. The term *geodesign* refers to this exact process of design and planning on different scales that are affected by both geospatial information and, especially, geospatial technology (Dias, Lee & Scholten 2014; Steinitz 2016). Geodesign is a way for administrators, leaders, and scientific professionals that are not necessarily well-versed in the practical possibilities or the functions of a GIS to benefit from spatial data and technology.

This study directly serves as an example of the potential for implementation in geodesign as a benefit to environment and industry alike (Huang 2016; Li 2016; Steiner 2016). While this study focuses primarily on the most accurate classification and mapping approach possible for a single set of surface materials, the resulting spatial data is directly useful for planning and

visualization of an ever-growing problem (Huang 2016). With a supplemental methodology, the automated classification for surface mines tested in this study could be used to predict the impact from toxic elements and mine drainage on human populations around the study area (Li 2016). Different factors originating from the surface mine classification data directly impact neighboring population centers, and are extremely useful for urban design approaches and strategic planning when it comes to health care, emergency preparedness, and water treatment.

5.1 Future Work

For all of these strategic applications, an adapted methodology oriented towards geodesign utilization that encompasses the classification used in this study would serve as an extraordinarily useful tool. What follows is a hypothetical methodology that could be used to take the automated classification representing surface mine pilings rich in ferric minerals and estimate the potential impact on both existing populations and built-up areas, as well as potential sites for new development. For this hypothetical methodology, the impact would be gauged solely in terms of water pollution impact. Water pollution impact in the instance of mine valley fills is created by pH imbalance and acidification created by introduction of ferric minerals to stream networks.

The hypothetical extended methodology is designed as a model in a GIS such as Esri ArcGIS. The inputs are: (1) the polygon feature class representing surface mines; (2) a detailed elevation model representing height of specific geographically referenced points in a grid above a standard ellipsoid or sea level; (3) a stream and river network polyline feature class with attribute information relating to flow volume and status as permanent or intermittent stream, as well as potential as source for drinking water; and finally, (4) a polygon feature class representing population (such as US Census district blocks that would suffice for the purposes of

such an impact study). A flow direction analysis processed with the elevation model as input would indicate (from every geographically referenced point in the study area) which direction water would flow. Streams would be hypothesized based on the elevation model, but the primary benefit for the flow direction model output would be identifying which surface mine pilings are in proximity of streams in the local drainage network. For an example of a simple flow direction output that represents a small sample area in the study area analyzed in this project, see Figure 19. The raster representation in the sample area shows the elevation values for raster cells on the left, and associated coded values output from the flow direction model on the right. Flow direction classifications refer to the direction that the ground is sloped, according to the *D8* model. This model assigns integer values of 1 to 8 depending on the direction the ground is sloped in relation to each cell's neighbors. For example, a value of 1 represents sloping due east, and a value of 8 represents sloping to the southeast (Jenson and Domingue 1988). Streams would then be coded in the hypothetical flow model based on a value derived from the size of nearby mineral pilings and the distance of these pilings from the stream in question. Coded values would aggregate as streams merge and approach population centers. Although this is not a perfect representation of the impact of acidification from multiple mineral pilings draining with rainfall into streams over distance, for this hypothetical workflow, it adequately represents the proportional extent of impact from multiple mines that may be closer or further from a stream that is downhill.

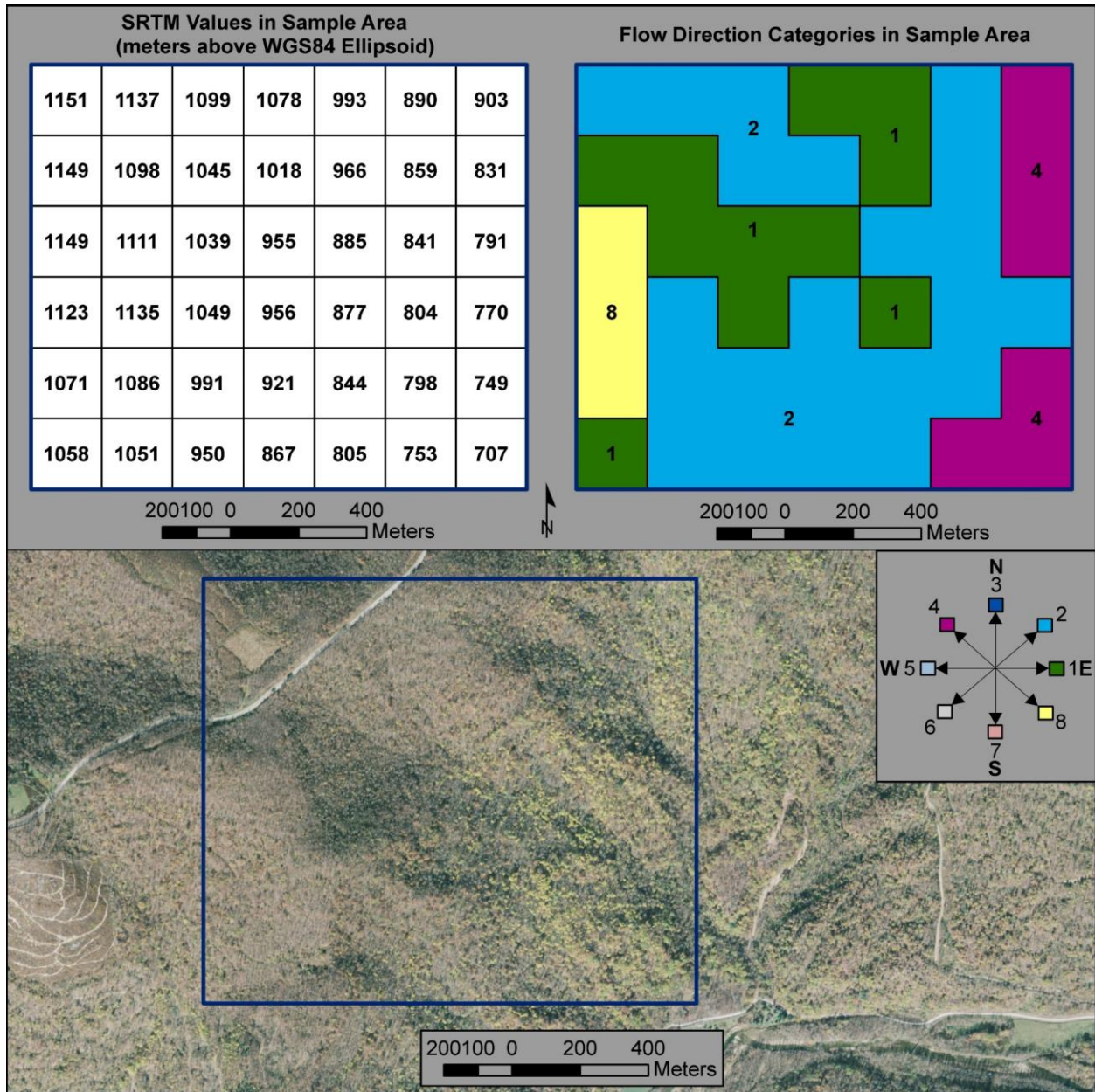


Figure 19 Subset of study area with representation of elevation values and flow directions

To conclude this hypothetical example of a methodology that would apply an effective and automated surface mine classification to geodesign principles, the codified stream network would then be related to population feature data. Streams that traverse densely populated districts that have a greater weight in terms of the value assigned from surface mine pilings and flow

would be highlighted, and the intersecting districts would be output in a separate polygon feature class for analysis. These districts are “at risk” in the sense that they are traversed by contaminated streams, and should be emphasized as targets for cleanup and treatment efforts. For areas with the highest population levels that are traversed by highly contaminated streams (as determined by the classification and subsequent flow model), the surface mine pilings themselves should be targeted for cleanup efforts upstream. A great deal of practical, strategic planning can be implemented with a methodology such as this flow model that can effectively and accurately predict impact on health and wellbeing for downstream populations.

5.2 Further Research

The accuracy of this study was rigorously tested, with 52 known mines active from 2000 to 2011, cross-referenced in terms of proximity to polygons classified as surface mine pilings in the automated classification. As 51 of these active mines were correctly identified, and with numerous inactive mines identified as well, the study was able to demonstrate rigor and thoroughness in satisfying scientific accuracy. The only concern remaining for the ability of the classification methodology to be deployed and applied broadly to map surface mines around the world are considerations pertaining to the terrain used in the study area.

While surface mines around the world focus on the same basic minerals being exploited in the study area in West Virginia (such as coal and copper), the terrain and image scenes collected in these areas do not. For example, areas of North Africa close to the equator have an extremely similar prevalence of both small and large scale surface mines. However, the surrounding terrain is predominantly sand and rock, instead of the forested and grassy areas that make up the image scene used in this study. To completely satisfy scientific rigor, and to confidently deploy this methodology for global application, an additional study in which

AVIRIS or similar hyperspectral data collected over an area with dense mining activity should be analyzed with the same automated mine classification methodology used in this study. From this, the results should be measured in terms of proximity to known active mine locations.

While the anticipated results of this follow-up study in a desert terrain environment would be similar to the results of this thesis project, there may be discrepancies resulting from the differences in soil types and vegetation with which the minerals targeted in the classification are mixed. The automated classification methodology normalizes the results so that mixtures are taken into account and only high concentrations of minerals typical of mine surface pilings and valley fills are classified. Conceivably, false returns or scattered light may result from high concentrations of sand and certain rock.

5.3 Applications of Research

The methods and results of this study offer the potential for practical application in real-world deployment through applications conducted with amended methodologies. Real-world applications involve collecting and processing hyperspectral image datasets (such as AVIRIS data) in an area where mapping of surface mines is required. The collection and processing of these data are the most time and resource-intensive processes. One significant consideration in this study is the expense of collecting new datasets. The data used in this study was collected and provided by NASA as a part of their research. The primary limitation of the findings from this study is that new collections are extremely expensive due to the costs of aircraft, fuel, crew, and the costly AVIRIS sensor itself. According to the USGS Spectroscopy fact sheet (sourced at <https://speclab.cr.usgs.gov/aboutimsp.html>), these costs amount to an average of \$64,000 per flight and \$6,000 per flight hour, not counting the initial costs of establishing a flight program. These costs are prohibitive for many potential users of surface mine classification, such as

private companies and governments of developing nations. However, the primary goal of this study was to test a methodology that could potentially be applied to raster spatial data irrespective of cost. Given the accuracy that was found in the methodology tailored for this study and for mapping surface mines, the algorithm and approach used is an ideal tool to have available as the cost of hyperspectral scanners and data collection is reduced in the future. Furthermore, studies such as this that demonstrate the efficacy of geoprocessing algorithms performed on hyperspectral data may help in motivating further development and widespread adoption of hyperspectral image collection and use.

This methodology can be employed without further development in both the United States and abroad to obtain a clearer picture of the spatial distribution of surface mines, and more importantly, of the toxic footprints they leave behind (Gurram 2016). During the research and data aggregation stages of this study, comprehensive mine feature classes were required in order to validate any classification results that were produced. While the federal OSM database contained detailed point information for mines in the state of West Virginia, detailed polygon feature classes representing mine footprints or valley fills do not exist. Such areas have been mapped in detail, but the polygon feature classes do not provide statewide coverage. In many states, they do not exist for any subset of the state. In West Virginia, mapped valley fill spatial data exist along the Western border, but no data is available for the study area. The automated classification tested in this study could provide such feature data with a minimum of user or analyst input, in addition to providing probable mine locations in areas that might not have even point feature data representing sites. In developing countries that often face graver hazards to human and environmental health as a result of mining operations, spatial databases and geoportals containing any type of mine feature data do not exist (Huang 2016). This

methodology would be able to provide valuable information representing the extent of mining operations in developing nations which could additionally help administrators and leaders visualize the impact of these operations.

The methodology employed in this study could easily be modified to accomplish a wide range of tasks in mapping and operational management. On a large scale, focusing on a particularly small and clearly defined area (such as a single industrial mining operation), a spectral scanner mounted on a drone could take layered image photographs of such a site at regular periods. If these hyperspectral scanned layers are georeferenced and classified at periods such as every week, the ongoing progress of a surface mine, as well as its impact on the surrounding environment, could be readily mapped and monitored by management.

Another potential project would utilize multiple *flight lines* or swaths of raster data collected under the aircraft scanner to create a wide area map of a larger site. Such a site that would benefit tremendously from obtaining comprehensive and up-to-date surface mine mapping would be a developing country that has no such data currently available (Huang 2016). An input dataset for the automated surface mine classification can take any size, and the only change in terms of processing would be time, which increases linearly with the number of raster cells or pixels present in the data (Fourest 2012). While developing nations would benefit tremendously from having a baseline feature spatial dataset representing surface mines and their footprints, highly developed nations with legacies of industrial mining (such as the United States and Australia) would also stand to benefit. Existing mine feature data and impact data could be updated, and in vast areas where no such polygon geometric feature data exists, foundation geospatial data could be created.

Another application of the methodology developed for this study is a hyperspectral classification of other materials, as pre-defined in a spectral library such as the JPL spectral dataset referenced for this study. Surface materials (such as concrete and water) were already precisely identified from returns in automated AVIRIS classifications as a stage of development in the methodology of this study (Clark 1990; Clark 1999; Dalton 2004; Rockwell 2005). These carefully identified hyperspectral signatures could be used individually or as a group to classify concrete and water in another hyperspectral image dataset. Other elements could be targeted and mapped with the same accuracy as was demonstrated in this study. A comprehensive classification effort could iterate through identifying raster fitting and depth layers for each element in a long list, and for each mineral produce output binary raster layers. The difference between a methodology that classifies and maps multiple elements that comprise features (such as surface mine pilings) and individual minerals is that the output from an individual mineral classification would be composed of multiple feature types. While the output of the surface mine classification was a single type polygon feature class, the output of an individual mineral map would have a class for each element (Clark 1999). As such, the final binary raster layers for each individual Earth element would need to be added by raster calculation one at a time, and combined values would be designated as an area of high concentration of specific, multiple mineral elements.

Such an application of a similar mapping methodology would be of significant use to mining companies and energy exploration companies. Being able to precisely identify and target both rare and common minerals based on soil composition on the Earth's surface would drastically reduce errors and redundancy costs in identifying new targets for exploitation. In the defense sector, a similar type of methodology for hyperspectral image classification that is

performed quickly and accurately could be employed to identify chemicals and mission targets as part of an Intelligence, Surveillance and Reconnaissance (ISR) effort. For example, as a part of drug interdiction efforts, specific plants and chemicals could be targeted and mapped reliably by low-flying aircraft collecting imagery with a hyperspectral scanner. In support of the warfighter and in support of troop protection efforts, explosive materials and unexploded ordnance (UXO) in given Areas of Operation (AOs) could be identified by an adapted methodology using georeferenced hyperspectral scans as input.

REFERENCES

- Adep, Ramesh Nityanand, Aswin P. Vijayan, Amba Shetty, and H. Ramesh. 2016. Performance evaluation of hyperspectral classification algorithms on AVIRIS mineral data. *Perspectives in Science* 8 : 722-6.
- Ahern, Melissa M., Michael Hendryx, Jamison Conley, Evan Fedorko, Alan Ducatman, and Keith J. Zullig. 2011. The association between mountaintop mining and birth defects among live births in central appalachia, 1996–2003. *Environmental Research* 111(6): 838-46.
- AVIRIS Image Cube. (2016) Retrieved October 20, 2016, from <http://aviris.jpl.nasa.gov/html/aviris.cube.html>
- Berge, A., A. C. Jensen, and A. H. S. Solberg. 2007. Sparse inverse covariance estimates for hyperspectral image classification. *IEEE Transactions on Geoscience and Remote Sensing* 45 (5): 1399-407.
- Bernhardt, Emily S., Brian D. Lutz, Ryan S. King, John P. Fay, Catherine E. Carter, Ashley M. Helton, David Campagna, and John Amos. 2012. How many mountains can we mine? assessing the regional degradation of central appalachian rivers by surface coal mining. *Environmental Science & Technology* 46 (15): 8115.
- Blahwar, B., Srivastav, S. K., & de Smeth, J. B. (2012). Use of high-resolution satellite imagery for investigating acid mine drainage from artisanal coal mining in north-eastern india. *Geocarto International*, 27(3), 231-247.
- Burns, Shirley Stewart, and American Council of Learned Societies. 2007. *Bringing down the mountains: The impact of mountaintop removal surface coal mining on southern west virginia communities, 1970-2004*. 1st ed. Vol. 5.;5;. Morgantown, W.Va: West Virginia University Press.
- Butler, Tom, 1963, and George Wuerthner. 2009. *Plundering appalachia: The tragedy of mountaintop-removal coal mining*. San Rafael, CA: Earth Aware.
- Canty, Morton John. 2014. *Image analysis, classification and change detection in remote sensing: With algorithms for ENVI/IDL and python*. Third ed. New York: CRC Press.
- Charou, E., Stefouli, M., Dimitrakopoulos, D., Vasiliou, E., & Mavrantza, O. D. (2010). Using remote sensing to assess impact of mining activities on land and water resources. *Mine Water and the Environment*, 29(1), 45-52.
- Clark, R.N., A.J. Gallagher, and G.A. Swayze, 1990, Material absorption band depth mapping of imaging spectrometer data using a complete band shape least-squares fit with library reference spectra, Proceedings of the Second Airborne Visible/Infrared Imaging Spectrometer (AVIRIS) Workshop. JPL Publication 90-54, 176-186.

Clark, R.N., G.A. Swayze, A. Gallagher, N. Gorelick, and F. Kruse, 1991, Mapping with imaging spectrometer data using the complete band shape least-squares algorithm simultaneously fit to multiple spectral features from multiple materials, Proceedings of the Third Airborne Visible/Infrared Imaging Spectrometer (AVIRIS) Workshop, JPL Publication 91-28, 2-3.

Clark, R.N., 1999, Spectroscopy of rocks and minerals, and principles of spectroscopy, in Rencz, A.N., ed., Remote sensing for the earth sciences, in Ryerson, R.A., ed., Manual of remote sensing, Volume 3: New York, John Wiley, p. 3-58.

Clayton, Janet L., Shelly A. Miller, and Raymond Menendez. 2015. In-situ bioassay response of freshwater mussels to acid mine drainage pollution and its mitigation. *Southeastern Naturalist*: 261-75.

Dalton, J. Brad, Dana J. Bove, Carol S. Mladinich, and Barnaby W. Rockwell. 2004. Identification of spectrally similar materials using the USGS tetracorder algorithm: The calcite–epidote–chlorite problem. *Remote Sensing of Environment* 89 (4): 455-66.

Dalton, J.B., Bove, D.J., Mladinich, C.S., and Rockwell, B.W., 2007, Imaging spectroscopy applied to the Animas River watershed and Silverton caldera, in Church, S.E., von Guerard, P., and Finger, S.E., eds., Integrated investigations of environmental effects of historical mining in the Animas River watershed, San Juan County, Colorado: U.S. Geological Survey Professional Paper 1651, pp. 143-159.

Dutta, Debsunder, Allison E. Goodwell, Praveen Kumar, James E. Garvey, Robert G. Darmody, David P. Berretta, and Jonathan A. Greenberg. 2015. On the feasibility of characterizing soil properties from AVIRIS data. *IEEE Transactions on Geoscience and Remote Sensing* 53 (9): 5133-47.

Fourest, Sébastien, and ebrary. 2012. *Satellite imagery: From acquisition principles to processing of optical images for observing the earth*. Toulouse, France: Cépaduès Éditions.

Gurram, Prudhvi, Heesung Kwon, and Charles Davidson. 2016. Coalition game theory-based feature subspace selection for hyperspectral classification. *IEEE Journal of Selected Topics in Applied Earth Observations and Remote Sensing* 9 (6): 2354-64.

Heinzel, V., Franke, J., & Menz, G. (2006). Assessment of cross-sensor NDVI-variations caused by spectral band characteristics. Paper presented at the Geoscience and Remote Sensing Symposium, 2006 , 6298(1) doi:10.1117/12.680278

Hendryx, Michael, and Benjamin Holland. 2016. Unintended consequences of the clean air act: Mortality rates in appalachian coal mining communities. *Environmental Science and Policy* 63 : 1-6.

Huang, Guoping, and Nianxing Zhou. 2016. Geodesign in developing countries: The example of the master plan for wulingyuan national scenic area, china. *Landscape and Urban Planning* 156 : 81-91.

Jenson, S. K., and J. O. Domingue. 1988. "Extracting Topographic Structure from Digital Elevation Data for Geographic Information System Analysis." *Photogrammetric Engineering and Remote Sensing* 54 (11): 1593–1600.

Jin, Song, Paul H. Fallgren, Jeffrey M. Morris, and Jeffrey S. Cooper. 2008. Source treatment of acid mine drainage at a backfilled coal mine using remote sensing and biogeochemistry. *Water, Air, and Soil Pollution* 188 (1): 205-12.

Joshi, P. K., Kumar, M., Midha, N., Yanand, V., & Wal, A. P. (2006). Assessing areas deforested by coal mining activities through satellite remote sensing images and gis in parts of korba, chattisgarh. *Journal of the Indian Society of Remote Sensing*, 34(4), 415-421.

John, D.A., Rockwell, B.W., Henry, C.D., and Colgan, J.P., 2010, Hydrothermal alteration of the late Eocene Caetano ash-flow caldera, north-central Nevada: a field and ASTER remote sensing study, in 2010 Symposium Volume: Geological Society of Nevada, Reno, Nevada, May 14-22, 2010, pp. 1055-1083.

Khalil, A., L. Hanich, R. Hakkou, and M. Lepage. 2014. GIS-based environmental database for assessing the mine pollution: A case study of an abandoned mine site in morocco. *Journal of Geochemical Exploration* 144 : 468.

Khalili, R., S. Anvari, and M. Honarmand. 2015. combination of biochemical and hyperspectral remote sensing methods for detection of heavy metal pollutions in eucalyptus leaves (case study: The city of bam). *The International Archives of Photogrammetry, Remote Sensing and Spatial Information Sciences* XL (1): 379-85.

Kruse, F. A., A. B. Lefkoff, and J. B. Dietz. 1993. Expert system-based mineral mapping in northern death valley, California/Nevada, using the airborne Visible/Infrared imaging spectrometer (AVIRIS). *Remote Sensing of Environment* 44 (2): 309-36.

Lambert, Hilary A. B. 2016. Whose water is it? *American Journal of Economics and Sociology* 75 (3): 681-720.

Lee, Danbi J., editor, Eduardo Dias editor, and Henk J. Scholten editor. 2014. Geodesign by integrating design and geospatial sciences. 2014th ed. Vol. 111.;111;. Cham: Springer.

Li, Weimin, and Lee-Anne Milburn. 2016. The evolution of geodesign as a design and planning tool. *Landscape and Urban Planning* 156 : 5-8.

Li, Yue, Hongli Zhao, and Jinghui Fan. 2015. Application of remote sensing technology in mine environment monitoring. *MATEC Web of Conferences* 22 : 4008.

Mars, John C., and James K. Crowley. 2003. Mapping mine wastes and analyzing areas affected by selenium-rich water runoff in southeast idaho using AVIRIS imagery and digital elevation data. *Remote Sensing of Environment* 84 (3): 422-36.

Rockwell, B.W., 2012, Description and validation of an automated methodology for mapping mineralogy, vegetation, and hydrothermal alteration type from ASTER satellite imagery with examples from the San Juan Mountains, Colorado: U.S. Geological Survey Scientific Investigations Map 3190, 35 p. pamphlet.

Rockwell, B.W., McDougal, R.R., and Gent, C.A., 2005, Remote sensing for environmental site screening and watershed evaluation in Utah mine lands: East Tintic Mountains, Oquirrh Mountains, and Tushar Mountains: U.S. Geological Survey Scientific Investigations Report 2004-5241, 84 p.

Steiner, Frederick R., and Allan W. Shearer. 2016. Geodesign—Changing the world, changing design. *Landscape and Urban Planning* 156 : 1-4.

Steinitz, Carl. 2016. On change and geodesign. *Landscape and Urban Planning* 156 : 23-5.

Yao-hua, Luo, Guo Ke, Tao Zhong-ping, and Wang Mao-zhi. 2012. The application research of hyperspectral remote sensing technology in tailing mine environment pollution supervise management

Zhang, B., Wu, D., Zhang, L., Jiao, Q., & Li, Q. (2012). Application of hyperspectral remote sensing for environment monitoring in mining areas. *Environmental Earth Sciences*, 65(3), 649-658.